Study of flash pyrolysis and combustion of biomass powders using the Godbert-Greenwald furnace: an essential step to better understand organic dust explosions

Matteo Pietraccini[1], Peter Badu[1], Theo Tait[2], Pierre-Alexandre Glaude[1], Anthony Dufour[1], Olivier Dufaud[1,*]

** Corresponding author: olivier.dufaud@univ-lorraine.fr*

[1] *Université de Lorraine, CNRS, LRGP, F-54000 Nancy, France*

[2] *Department of Chemical & Process Engineering, University of Strathclyde, G11XQ Glasgow, Scotland, United-Kingdom*

Abstract

An organic dust explosion is a heterogeneous system on a space and time scale. Predicting the parameters characteristic of its severity needs experimental and theoretical approaches to find the optimal compromise between consistency with reality and modelling time. A hybrid method is proposed to study flash pyrolysis and combustion of several organic powders (cellulose, wheat starch, oak wood, Douglas fir and olive pomace). A Godbert-Greenwald furnace was employed to perform the experiments to mimic the fundamental characteristics of a dust explosion: high particle heating rate, high reaction temperature and short residence times. At 973K, the residence time is a critical parameter: the large particles of cellulosic compounds (wood, cellulose) do not reach their pyrolysis temperature and only fibres smaller than 20 or 30 µm are fully converted. As the particle size distribution of starch is smaller, heat transfer is not directly the limiting phenomenon but rather the strong tendency

This is a peer reviewed, accepted author manuscript of the following research article:
Pietraccini, M., Badu, P., Tait, T., Glaude, P-A., Dufour, A., & Dufaud, O. (2023).
Study of flash pyrolysis and combustion of biomass powders using the Godbert-Greenwald furnace :
an essential step to better understand organic dust explosions. Process Safety and Environmental Protection, 169, 458-471.
https://doi.org/10.1016/j.psep.2022.11.041

for powders to agglomerate during pyrolysis. At higher temperatures, secondary reactions of primary tars are evidenced, stressing the influence of the pyrolysis stage and leading to heterogeneous combustion. The composition of the pyrolysis gases as a function of the nature of the powder and the temperature was also determined. A lumped-kinetic model adapted to dust explosion was developed and validated for cellulose. The kinetics constants corresponding to levoglucosan to permanent gases and cellulose to char and water reactions are significantly different from those proposed by the literature, demonstrating that dust explosion kinetic parameters must be obtained under conditions consistent with such phenomenon.

Keywords: Pyrolysis, oxidation, organic powder, dust explosion

Graphical abstract

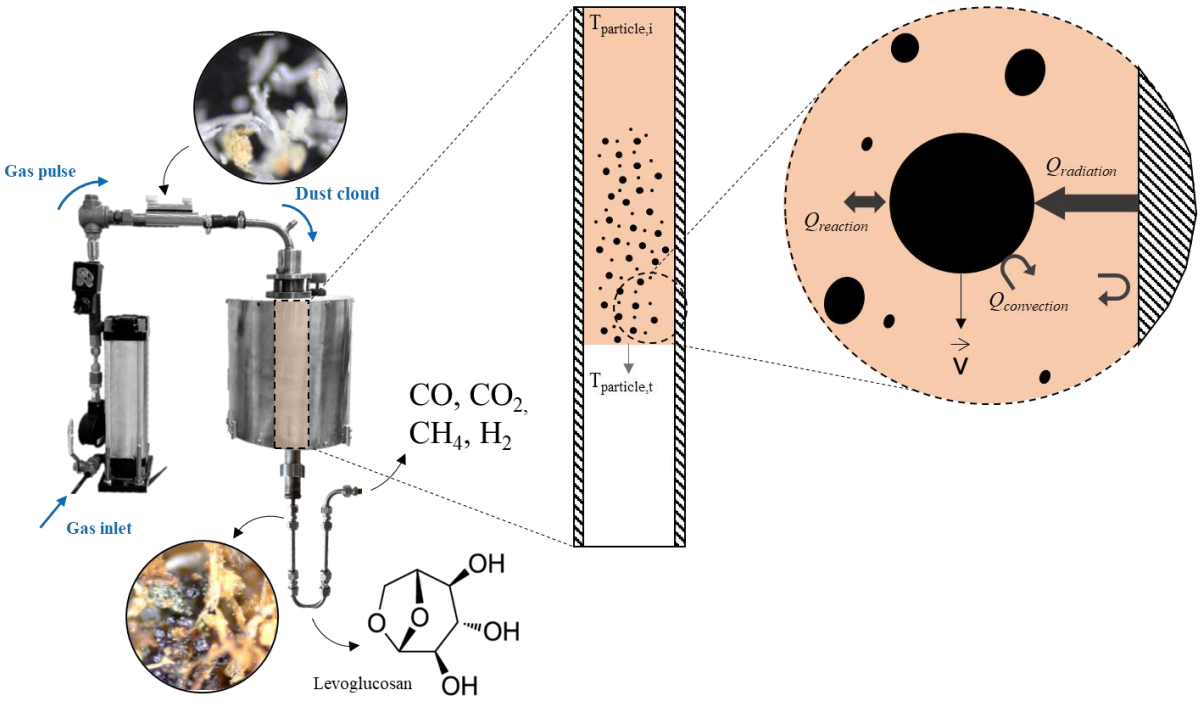

1. Introduction

The answer to the "simple" question asked by an industrialist or a health and safety officer "Can you predict the consequences of an explosion of this specific powder?" is far from obvious. Rephrasing this request, it means to ensure that, under all operating conditions of a process, it is possible to quantitatively evaluate the explosion severity of a product. A response based on a study performed only under standard conditions, although necessary, would not allow the diversity of industrial conditions encountered to be considered and reproduced.

Moreover, an exclusively experimental response would require a costly and time-consuming multiplicity of tests. Similarly, the use of modelling, although potentially associated to an appropriate and relevant response, could not be successful without preliminary testing. For instance, Islas et al. [1] proposed a three-layer method to study biomass dust explosions: by merging the CFD simulation of the dispersion process, ignition and flame propagation steps, experimental tests and general knowledge of the chemical mechanisms involved, it is possible to deepen the conclusions that may be drawn from an explosion experiment.

However, modelling a dust explosion means considering an impressive number of phenomena, some occurring in parallel, others in series, and all subject to complex interplays. In the case of an organic powder dispersed in air, it is necessary to consider, among others, the preheating of the particles (external radiation and convection, internal conduction), the pyrolysis stage, the mass transfers of gases (air-to-particle and pyrolysis gases-to-ambient gaseous phase), the oxidation reaction, the hydrodynamics of the flame, and the heat transfer

from the flame. To study experimentally and independently each of these stages is illusory as they are interdependent. On the other hand, it seems relevant to dissect the explosion into simpler stages: particles heating, pyrolysis and oxidation to better model these three main phenomena. For each of these steps, it is important to estimate their characteristic times, the products involved and to propose global kinetic models.

The operating conditions play an essential role for these three phenomena, and it is therefore required to keep them identical, or at least very close, to what happens during a dust explosion. Therefore, thermogravimetry analysis (TGA), differential thermal analysis (DTA) or differential scanning calorimetry (DSC) are essential resources to study the thermal stability of powders. However, they cannot be used to mimic the reactions of particles dispersed in air, since the heating rate is greatly different. The ideal solution would be to study these explosions on site, under industrial conditions, but this is neither possible nor desirable. At the other end of the spectrum of potential solutions, focusing on the behaviour of a single particle subjected to rapid heat flux, even if this approach offers many advantages, omits all the particle-particle interactions that inevitably occur during an explosion. Finally, a 20 L explosion sphere, a standardised tool accessible in many process safety laboratories (ISO/IEC 80079-20-2 standard), does not, in its original state, allow either the study of the heating and pyrolysis stage or the rapid variation of the initial temperature of the particle cloud over a temperature range consistent with the pyrolysis stage, i.e. more than 300°C. Given these considerations, the use of the Godbert-Greenwald (G-G) furnace to study the constituent steps of a dust explosion appears to be an interesting alternative, although not unique.

Several works exploited such apparatus for its simplicity and its versatility, for instance, to study complex explosible mixtures, such as coal-rock dust binary mixtures [2] and carbonaceous dust clouds in presence of CH_4, H_2 and CO [3]. The influence of the G-G

furnace on the cloud particle size distribution was carried out by Bu et al [4], by identifying and quantifying the modification of characteristic diameters. Mittal et al. [5] worked on the influence of particle size and dust concentration on the MIT of polyethylene fibres. They focused on the identification of the values associated with the worst-case scenario in terms of ignition sensitivity. They later developed a model based on a thermal balance and a single reaction involved in the autoignition of the dust cloud [6]; the activation energy was equal to that of ethylene oxidation and the product of the oxidation enthalpy and reaction rate constant was computed from a single experiment data point. Chen et al. [7] compared three models for describing the ignition of a dust cloud in a G-G furnace, detailing the choice of the reaction kinetic parameters used in their work, but without considering the particle heating step. Xu et al. [8] focused on the determination of the MIT of coal dust and the kinetics of its combustion. Through thermogravimetry analyses (TGA) and the on-line analysis of the gaseous products, they showed that temperature and heating rate have an influence on the reaction rate. The operating conditions used in their work (heating rate, particle final temperature and sweeping gas) are nonetheless far from those typically encountered during an organic dust explosion. Finally, two models were proposed by Addai et al. [9] to estimate the MIT of hybrid mixtures. They also showed that the models previously proposed by Krishna, Cassel and Mitsui showed good agreement for pure dust [9]. However, the thermo-kinetic parameters were not made explicit and needed to be fitted, for each sample, from the MIT experiments.

The approach chosen here consists in identifying the rate-limiting step of the explosion of organic dusts and proposing a simplified mechanism associated to a kinetic law representing this reactional stage, through experiments performed under conditions similar to those of dust explosions. Coupled with heat balances similar to those described previously, this approach aims to develop reaction schemes specific to dust explosions and which would be adaptable to different operating conditions without having to resort to a systematic

adjustment of thermo-kinetic parameters. In addition, this approach assesses the composition of the gases generated during the pyrolysis and combustion phases, which provides information on the gas compounds to be considered for flame propagation models.

On theoretical and experimental grounds, a model for the particle heating as they fall through the Godbert-Greenwald furnace has been developed. The flash pyrolysis and combustion of five biomass powders were then studied at different temperatures using this apparatus. From the analysis of the collected gases, chars and tars, lumped kinetic mechanisms are proposed to model the constituent steps of the explosions.

2. Materials and Methods

The powders chosen were wheat starch, cellulose, oak, Douglas fir and olive pomace. The two first represented pure components. The lignocellulosic materials are known for being chemically complex. Their peculiar behaviour is mainly due to the numerous interactions between the three main components: cellulose, hemicellulose and lignin. Liu et al. [10] studied the explosion severity of several binary mixtures of these three and revealed an overall strong influence of cellulose and lignin on the explosion overpressure. At the same time, hemicellulose seemed to play a more significant role in the rate of pressure rise.

Due to their well-known chemical homogeneity and their abundance, cellulose and starch were chosen as the reference powder samples. The samples used in this study were microcrystalline cellulose from DuPont (Avicel PH-101).

Starch is the third most abundant biopolymer, behind only cellulose and chitin. It is broadly classified into three groups based on its origin: type A (from cereals), type B (from tubers, fruits and stem) and type C (from legumes and roots) [11]. In this work, a type A starch (from wheat) was purchased from Sigma Aldrich.

Due to the current growing interest in biomass, three lignocellulosic materials were chosen for this study: Douglas fir (softwood), oak (hardwood) and olive pomace. The first two are woody biomasses harvested in the Haut-Beaujolais region (France), while the third one represents an abundant waste product in Mediterranean countries. The wood samples were initially chunked into small-sized chips, excluding the bark, followed by knife milling (Retsch SM 300) at 1500 rpm. Powdered samples were later sieved for 5 minutes in an AS 200 vibratory shaker with 180 and 56 µm sieves.

The increasing heterogeneity of these five samples was meant to compare the fast oxidation of a pure component (such as cellulose and starch) to that of lignocellulosic materials, by subsequently adding complexity.

The particle appearance of the five powders was characterized by digital (a 5 Mp Dino-lite Pro HR digital microscope) and electronic imaging (JEOL JSM-649-LV Scanning Electronic Microscope or SEM) methods. Photos were also taken with a Canon 2000D to show their macroscopic appearance. The Particle Size Distribution (PSD) of the samples was determined by a Malvern Mastersizer 3000 equipped with an aero-dispersion unit.

Proximate analysis was performed on the five powders, determining their moisture content (MC), volatile matter (VM), fixed carbon (FC) and ash content. The MC was determined with a Mettler Toledo HE53 Moisture Analyzer: approximately 0.5 g of sample was placed in the apparatus and heated at 105°C for 15 minutes by an IR lamp, to determine the water mass loss and thus the humidity of the powder. VM and FC were calculated by thermogravimetric analysis (TGA) in a Mettler Toledo TGA STARe System. The temperature profile was: 105°C for 30 min, then 15 $K.min^{-1}$ up to 900°C, 10 min at 900°C under N_2 and finally 20 min under air at 900°C. This specific temperature profile (reported in Figure S 1 in the Supporting information) was used to determine the Volatile Matter (VM) and the Fixed Carbon (FC) of the selected powders. The volatile matter was calculated by subtracting the

mass of the sample at 40 min (when the curve reached a plateau after the dehydration step, at 105°C) and 100 min (when the flow gas was switched to air, at 900°C), and normalized by the mass at 30-40 min. By knowing the Moisture Content (MC), the volatile matter and the ash content, it was possible to calculate the fixed carbon content with the following formula:

$$FC = 100 - MC - VM - ash \quad (1)$$

By changing the carrier gas from nitrogen to air, it was possible to differentiate the VM from the FC. Moreover, by exploiting the curves obtained by thermogravimetric analysis, it was also possible to determine the pyrolysis onset temperature T_{onset}. The ash content was assessed with the aid of a Nabertherm B150 oven: samples were weighed, placed in the furnace, heated to 950°C for 4h and then weighted again. The ratio between the residual and the initial mass corresponds to the ash content.

2.1 *Modified Godbert-Greenwald furnace*

Experiments were carried out in a Godbert-Greenwald furnace, usually employed for the determination of the Minimum Ignition Temperature (MIT) of a dust cloud, according to the ISO/IEC 80079-20-2 standard [12]. The original G-G furnace was equipped with two coaxial Inconel cylinders to ensure its airtightness, and modified to offer the possibility to collect the products generated by both pyrolysis and combustion, i.e. the solid residues (char), condensable products (tar) and permanent gases. The experimental setup is schematised in Figure 1.

The powder was dispersed into the vertical tubular furnace by a gas pulse. Argon was used for the pyrolysis test, whereas air was used for the combustion tests. Before each test, the setup was flushed for approximately five minutes with argon to remove residual air and moisture. To check the airtightness of the apparatus, blank tests were performed without dust.

Oxygen and nitrogen concentrations in the collected gas were analysed by micro-Gas Chromatography (GC), considering the maximum allowable concentrations equal to 0.5 and 2 vol%, respectively. These last were imposed by the air tightness of the experimental setup, which did not allow a 0%-oxygen atmosphere to be reached. Placed just after the heated chamber, a double-layered round metallic 2 mm mesh (10 mm diameter) allowed to sample the solid residues. The condensable fraction was sampled in a U-shaped tube, which was externally cooled by isopropyl alcohol at -30°C (by mixing isopropanol with liquid N_2) in a Dewar. The gaseous products were collected in a collapsible Tedlar bag for analysis. To study the influence of the reactor temperature, experiments were performed at 700, 800 and 900°C. These temperatures (700, 800, 900°C) always refer the reactor wall temperature and not the particle temperature within the oven, which remains unknown. Several factors came into play to choose these temperatures:

- The MIT of the chosen organic powders (beyond which the combustion can occur);
- The small residence time of the dust cloud in the heated chamber (which must be coupled to temperatures high enough to allow the particles to heat rapidly);
- The exothermicity of the combustion phenomenon (whose contribution to the heating process leads to high flame temperature, which is no longer related to the reactor temperature);
- The maximum temperature that can be reached by the oven (950°C).

For each temperature, 0.2 g of sample was dispersed in the pre-heated chamber, to attain an average dust concentration in the heated chamber of about the stoichiometric value, associated to the combustion of the selected materials. The stoichiometric concentration depends on the powder nature but, since the actual dust concentration varies with time and space as a function of the operating conditions (injection pressure, residence time), it is illusory to adjust "precisely" the nominal concentration (mass of powder divided to the

furnace volume) with the theoretical stoichiometric concentration. Previous tests aiming at determining the minimum ignition temperature of the powders showed that the "most vigorous ignition" [12] was mainly obtained for the 0.2 g of sample. Moreover, larger amounts of powder would have led to significant deposits of unreacted powder inside the setup. Finally, the dust container was designed to allow the full dispersion of the powder (less than 10 wt% dust remaining in the container after injection).

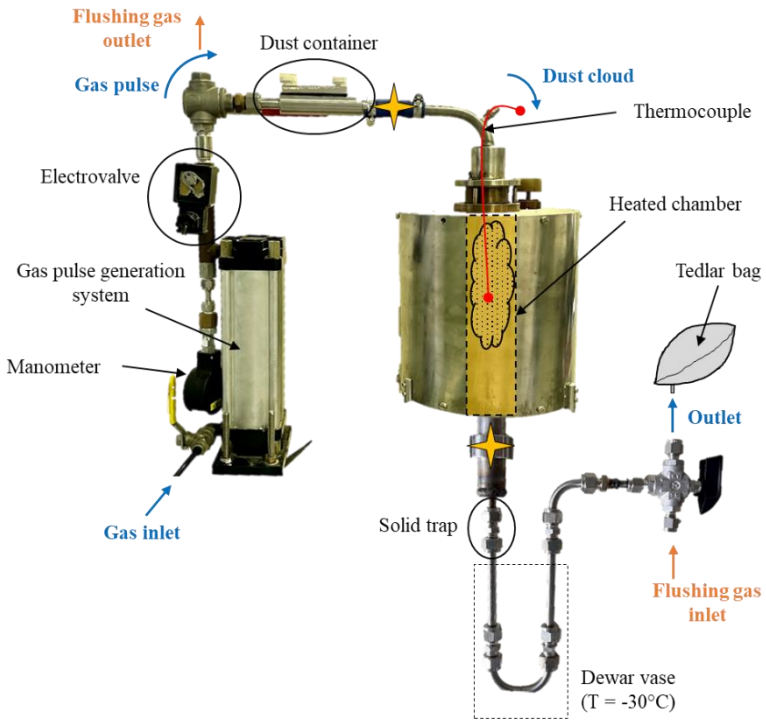

Figure 1 - The modified configuration of the Godbert-Greenwald furnace. The yellow stars indicate where the in-situ PSD analysis was performed.

The test procedure was repeated fivefold to obtain enough solid and condensable residues for the follow-on analyses. Gaseous products were analysed only for the first dispersion, to avoid contamination by the unreacted powder deposits from the previous dispersions.

The adequate residence time of the dust cloud was obtained by determining the optimum point between an efficient dispersion and enough high degree of conversion. The former is associated with the pressure pulse applied to ensure the dispersion of all the powder. The

latter is associated with the residence time of the particles in the reactor. These two factors are conflicting. A high-speed camera (Mikrotron MotionBLITZ Eo Sens mini, set to an acquisition rate of 200 fps) was employed to find the optimum gas pulse pressure value. It was placed in front of the experimental setup to record the dust cloud's inlet and outlet times, whose difference was used as an estimation of the average residence time of the dust cloud (MotionBLITZ Director2 operator software was used for the high-speed video treatment). By rapidly dispersing the powder samples into the vertical tubular furnace and varying the dispersion pressure (from 1.3 to 1.8 bars), dust residence times within the range of 150 - 200 ms were determined.

A dry in-situ dispersion study was also performed with a Helos laser diffraction sensor (Sympatec) at two different levels of the experimental setup (indicated by a yellow star in Figure 1). This analysis allowed to monitor the particle size distribution (PSD) of the dust cloud as well as the optical concentration as function of time. This analysis aimed to highlight the agglomeration phenomena of the powders, but also to estimate the residence time range associated to the highest concentration of particles. Analyses were performed thrice for repeatability purposes.

2.2 Thermal study of the dust cloud

After the dispersion, the dust cloud passes through the heated chamber and the temperature of the particles starts to rise. To distinguish and compare the heating and the reaction time, a heat transfer model was developed. Hence, the particle temperature profile along the vertical chamber was determined. Based on the procedure proposed by Piskorz et al. [13], the following particle heat balance was built:

$$\frac{1}{4}\pi d \qquad \text{—} \qquad . \qquad . \qquad .$$

$$- \qquad \frac{}{} \qquad L(T \qquad) \qquad L(T \qquad) \qquad -$$

where $\dot{q_{rad}}$ is the radiative heat transfer, $\dot{q_{reac}}$, the reaction heat contribution and $\dot{q_{con}}$, the convective or conductive heat transfer. The shape of the cellulose particles was approximated with a cylinder to consider its fibrous and elongated structure, associated with a diameter d_p and a length L.

The value of $\dot{q_{con}}$ can be adjusted as a function of the limiting heat transfer mode. If the Biot number Bi is greater than 1, the internal heat transfer limits the overall heat transfer; whereas if Bi is lower than unity, the particle conversion is limited by the external heat transfer and the particle is thus deemed "thermally thin". Calculations were done based on the physical properties of the cellulose sample.

$$\frac{}{} \quad - \quad \frac{(T \qquad)}{(T \qquad)}$$

Considering a wide range of particle (T_p) and furnace (T_w) temperatures, the convective Biot number is always lower than the radiative Biot number, which is lower than 0.2, as reported in Equation (3). In such a case, the particles are considered to have a uniform temperature, which is consistent with the study of Piskorz et al. [13].

According to the shrinking-core theory, the particle size decreases as the pyrolysis processes progress and, assuming a cylindrical particle, the following equation was added to the system:

$$\frac{d(d_p)}{} \qquad - \quad \left\{A \exp\left(- \frac{}{}\right)\right\} -$$

Equations (2) and (4) were solved simultaneously with Matlab (Mathworks), for the three selected wall temperatures. The values used for the calculations are reported in Table 1. The emissivity of Al_2O_3 ceramic (G-G furnace wall) is approximately 0.90, varying as a function

of the temperature. It is also the case of oxidized Inconel which was used as inner tube: its emissivity exceeds 0.8 as soon as the temperature reaches 600°C and reaches 0.88 at 900°C [14]. Therefore, the value chosen for the calculation was 0.9.

Table 1 - Parameters used for solving the particle heat balance system.

Parameter	**Value**	**Unity**	**Source**
dp	20 – 100 – 200	µm	Determined experimentally
ρ_s	700	$kg.m^{-3}$	Lédé et al. [15]
C_{ps}	1758	$J.mol^{-1}.K^{-1}$	Piskorz et al. [13]
F	1	-	Geometrical consideration
ε	0.9	-	Green et al. [14]
h	30	$W.m^{-2}.K^{-1}$	Dufour et al. [16]
ΔH_p	335	$J.kg^{-1}$	Piskorz et al. [13]
E_a	197300	$J.mol^{-1}$	Piskorz et al. [13]
A	$2.83 \cdot 10^{19}$	s^{-1}	Lédé et al. [15]

2.3 Product characterization

For all samples, a global mechanism composed of three steps was employed to describe the reactions involved: primary pyrolysis, secondary pyrolysis and oxidation. The products of the pyrolysis and combustion tests were characterized, to collect information concerning the three steps. This lumped multistep reaction scheme is represented in

Figure *2*.

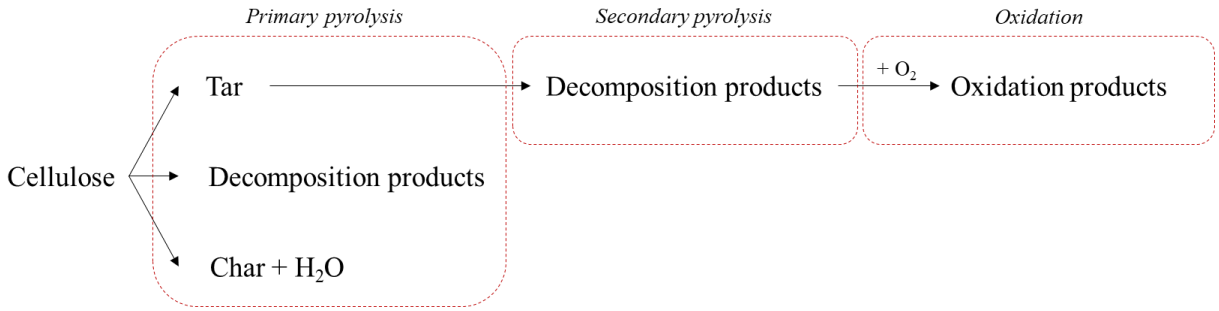

Figure 2 - Cellulose lumped combustion multistep mechanism.

2.3.1 Solid products

The solid products (partially converted biomasses) sampled by the trap after the heated chamber and were analysed using a 5 Mp Dino-lite Pro HR digital microscope and a JEOL JSM-649-LV Scanning Electronic Microscope. The information obtained was used to characterize their appearance, colour, shape and morphology.

Complementary information about the solid residues was obtained through FT-IR absorbance (Bruker Optics SARL Alpha P) and thermogravimetric analysis (Mettler Toledo, TGA - STARe System thermogravimetric balance). Between 6 and 10 mg of solid residue samples, collected at each temperature were heated from 30° to 950°C at 15°C/min. Experiments were conducted under a nitrogen atmosphere at 1 bar and with a 100 mL/min flowrate.

2.3.2 Condensable product characterization

The condensable fraction collected in the U-shaped tube after the heated chamber was rinsed and solubilized in methanol. 1 µL of 1-tetradecene was added as an internal standard, the solution was filtered with a 0.45 µm pore filter and analysed by a GC-MS, equipped with a FID detector (Agilent 7890A System equipped with a 5975C Triple-Axis detector). Results

were used to determine the most accurate tar-representing molecule in the pyrolysis step for the fast combustion model.

2.3.3 Gaseous product characterization

Pyrolysis and combustion gases were analysed by micro gas chromatography (SRA 3000 µGC equipped with a TCD detector, 3 ways). Permanent gases (CO, CO_2, CH_4, H_2, O_2 and N_2) were measured, as well as some aromatics (benzene, toluene and xylene isomers) and some light hydrocarbons (C_2H_2, C_2H_4 and C_2H_6).

2.4 Flash pyrolysis and fast combustion models

The aforementioned multistep reaction system (Figure 2) was used to describe the kinetic behaviour of the powders. Results concerning condensable and gaseous products were used to select the most abundant chemical species to be considered in the construction of this mechanism. The main objective of this model is to determine the kinetic parameters (activation energies and pre-exponential factors) of the selected reactions from experimental data.

3. Results and discussion

Figure 3 presents the appearance of the powder samples, as well as the colour, shape and surface morphology of the particles. SEM and digital images allowed to underline the importance of two main aspects: the shape of the particles and the heterogeneity of the samples. As for cellulose, oak and Douglas fir, the fibrous character conferred by the cellulose

chain results in elongated particles, in which the characteristic length for heat and mass transfer is most probably the thickness, i.e. the smaller dimension (between 20 and 50 µm for cellulose). Oppositely, wheat starch and olive pomace particles are associated with higher sphericity, in which the key length is the diameter. Moreover, from cellulose and starch to olive pomace, an increasing heterogeneity of the particles is noticeable.

Table 2 reports some characteristic diameters (D10, D50 et D90) and the pyrolysis onset temperature T_{onset} of the powder samples (obtained by the starting point of mass loss from TGA). Except for wheat starch, the PSD characteristic dimensions are in the same order of magnitude. Furthermore, as expected, the chemical nature of the powders seems to influence the pyrolysis onset temperature: as the complexity of the tested material increases (from cellulose to olive pomace), pyrolysis starts at lower temperatures. This can be associated with the higher reactivity of hemicelluloses and lignin compared to cellulose and to mineral catalytic effects.

Figure 4 shows the proximate analysis of the samples. Variations in the volatile matter (and thus in the fixed carbon) depend on the composition and content in lignin, cellulose and hemicellulose [12, 13, 14]. Yee Wen Chua et al. [20] mentioned a sensible discrepancy between the ratio VM/FC of cellulose and lignin, respectively equal to 10.9 and 1.3. Olive pomace presents a higher ash fraction which is mainly due to the contribution of the olive stone to the overall mineral content of this sample [21]. It was not possible to determine the volatile matter and fixed carbon fractions of wheat starch due to its tendency to form a foamy structure during the heating process, which was not compatible with the analysis in the thermo-balance.

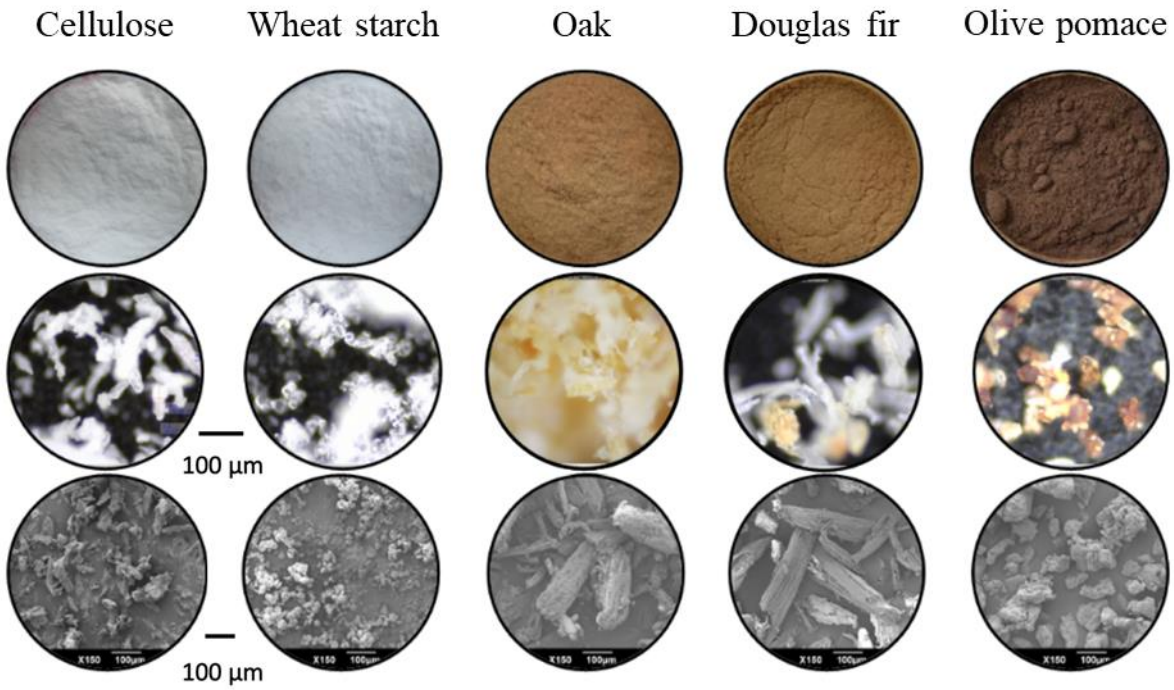

Figure 3 - Appearance (top-row), digital (middle-row) and SEM (bottom-row) images of the powder samples.

Table 2 - Characteristic PSD diameters and pyrolysis onset temperature of the samples.

Sample	**D10 (µm)**	**D50 (µm)**	**D90 (µm)**	**T_{onset} (°C)**
Cellulose	21	59	140	305
Wheat starch	12	20	33	-
Oak	20	51	107	264
Douglas fir	19	48	86	292
Olive pomace	24	59	102	176

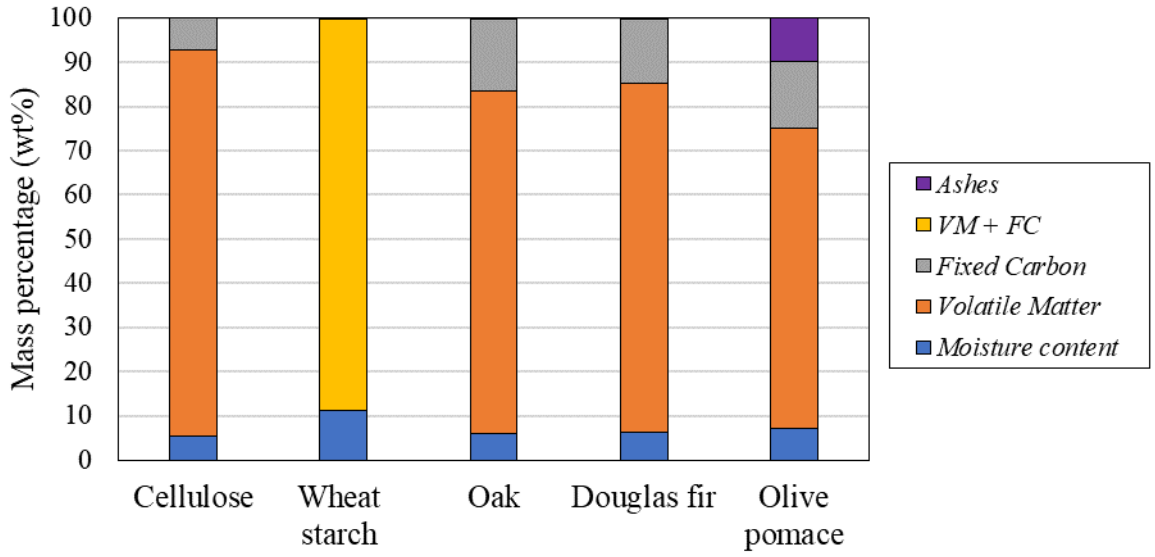

Figure 4 - Proximate analysis of the powder samples.

3.1 Dust cloud thermal study

The thermal evolution of a cellulose cloud in the G-G furnace was studied. Results are reported in

Figure *5* and Figure 6. The heating of the cellulose fibres is linear in time and then reaches a semi-plateau around 600-700K after triggering pyrolysis reactions. The pyrolysis onset temperature was determined experimentally around 578K for cellulose (as reported in Table 2), which is lower than the results obtained with the particle heat balance. Piskorz at al. *[13]* presented a similar particle temperature profile, with a plateau around 700-800K. The discrepancy with their work is likely due to the different reactor temperature (i.e. 1373K) and particle size (two sieved fractions of Avicel ph 102 were used in their work, significantly coarser than the Avicel ph 101 used in this work). The particle then decomposes in a quasi-isothermal way, which leads to the shrinking of the particle. As the fibre thins, its surface-to-

volume ratio increases, and both the radiative and convective heat transfer become more significant than pyrolysis. Thus, the particle temperature shows a slight increase.

For the temperature values considered (from 973 to 1173K), the time scale of the pyrolysis step is always higher than the one associated to the particle heating. The initial thickness of the cellulose fibres was set at 20, 100 and 200 µm to enlighten the diversity of the particle size in the dust cloud. A complete conversion of the particles may be attained between 160 and 1400 ms at 973K, and between 70 and 650 ms at 1173K. It clearly shows a considerable heterogeneity of the global conversion degree in space and time, which was expected for a highly heterogeneous system as a dust cloud.

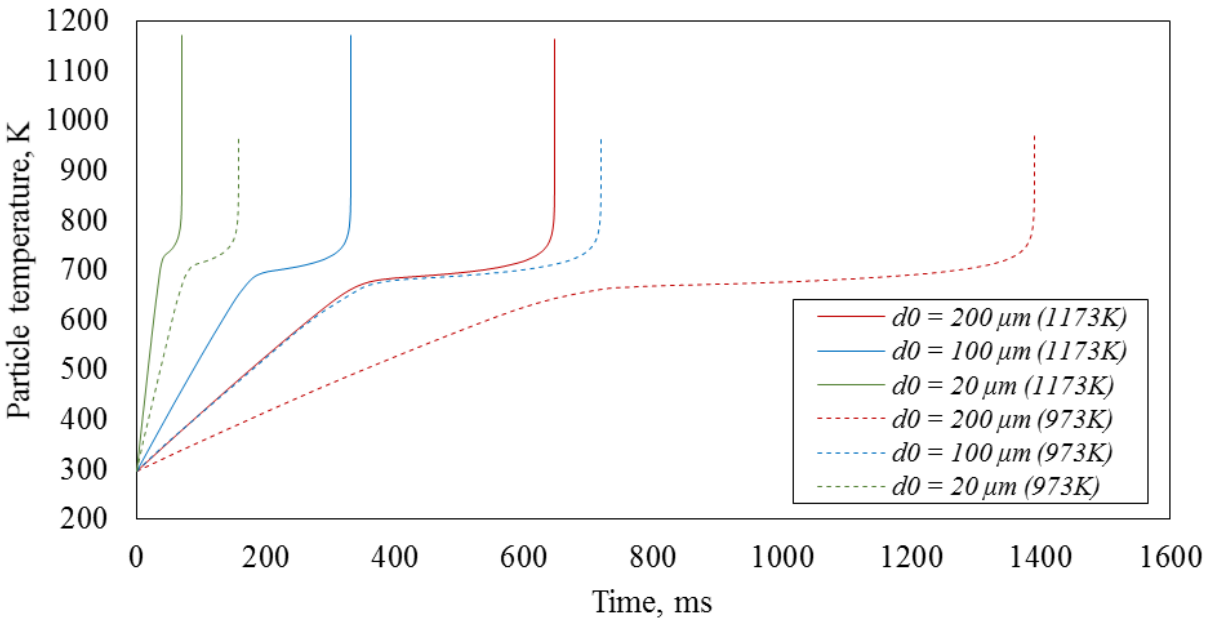

Figure 5 - Time-evolution of the particle temperature when exposed to a set temperature in the G-G furnace.

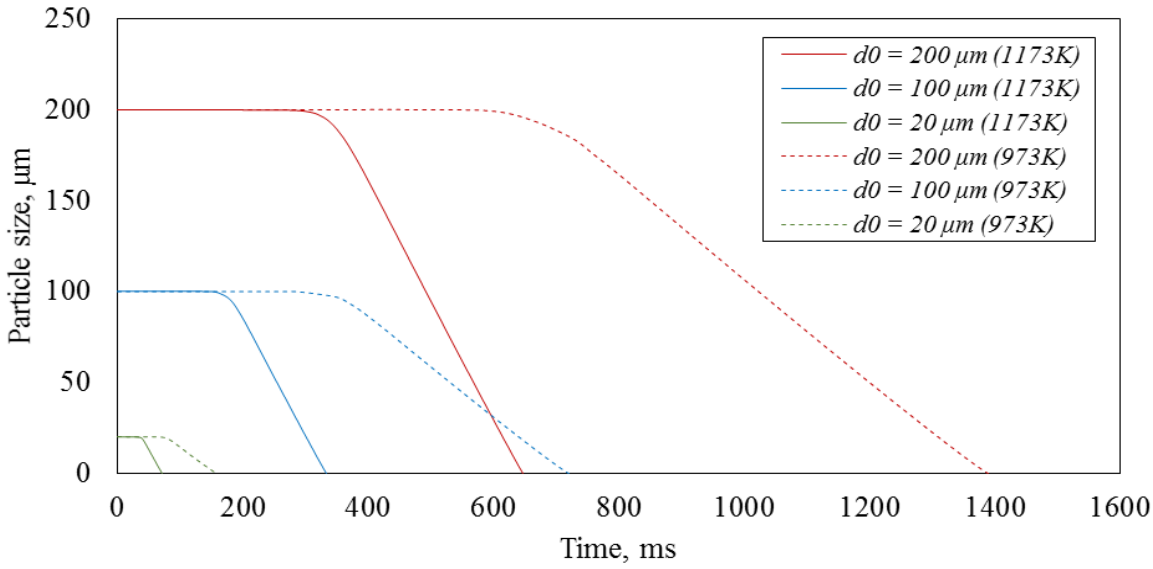

Figure 6 - Time-evolution of the particle size when exposed to a set temperature in the G-G furnace

The literature provided scattered values for the pyrolysis reaction enthalpy. Since it is a crucial parameter for the particle heat balance, a sensitivity analysis was carried out to determine its influence on the profiles reported in Figure 5 and Figure 6. Results are reported in Figures S 5, S 6, S 7 and S 8 in Supporting information.

Figure 7 reports the time evolution of the particle temperature and the optical concentration associated with the dust cloud passing through the heated chamber. The optical concentration was measured at the heated chamber's inlet and outlet, respectively referred to as "top" and "bottom". A high-particle concentration zone was identified between 0 and 300 ms, approximately. By overlapping the particle temperature profiles (calculated for an intermediate size of 100 µm at 973 and 1173K) and the optical concentration curves, it seemed that, even though particles reached the pyrolysis onset temperature before exiting the furnace, the quasi-isothermal plateau around 700K is attained only after.

The second layer of information is associated with the optical concentration, i.e. the extinction level of the laser sensor, which is proportional to the total volume of the particles

crossing the laser beam at a given time [22]. Focusing on the optical concentration associated with the dust cloud exiting the heated chamber (which is considered the most representative of the dust cloud inside the heated chamber), it is then possible to estimate the region where particles react and generate the products subsequently collected and analysed. Figure 7 shows that at 1173K, less than 75% of the 100 µm particles have a sufficiently long residence time in the Godbert-Greenwald furnace to reach their pyrolysis temperature. The study of the temporal evolution of the particle size distribution shows that the particles with the shortest residence time are agglomerates or large fibres (see Figure S 2, Figure S 3 and S 4 in Supporting information), mainly due to the inertial effect. These particles being characterized by a higher pyrolysis time scale. Hence, they exit the heated chamber only partially pyrolyzed. Figure 7 also shows that at a temperature of 973K, 100 µm particles would not reach the MIT until 83% of the powder has already left the furnace, which greatly limits the probability of propagation of the potentially created flame core. Previous authors had observed similar behaviours, but without characterising the residence times and particle size distributions. For example, Mishra and Azam [23] concluded that large coal particles were barely ignitable even at a temperature higher than 850 °C due to their low residence time in the G-G furnace. This experimental approach allows the determining of the actual residence time of each granulometric class and an estimation of the pyrolysis efficiency and thus, of an ignition likelihood. It should also enable to adjust the test parameters to the properties of the powders in a relevant manner for the determination of the MIT.

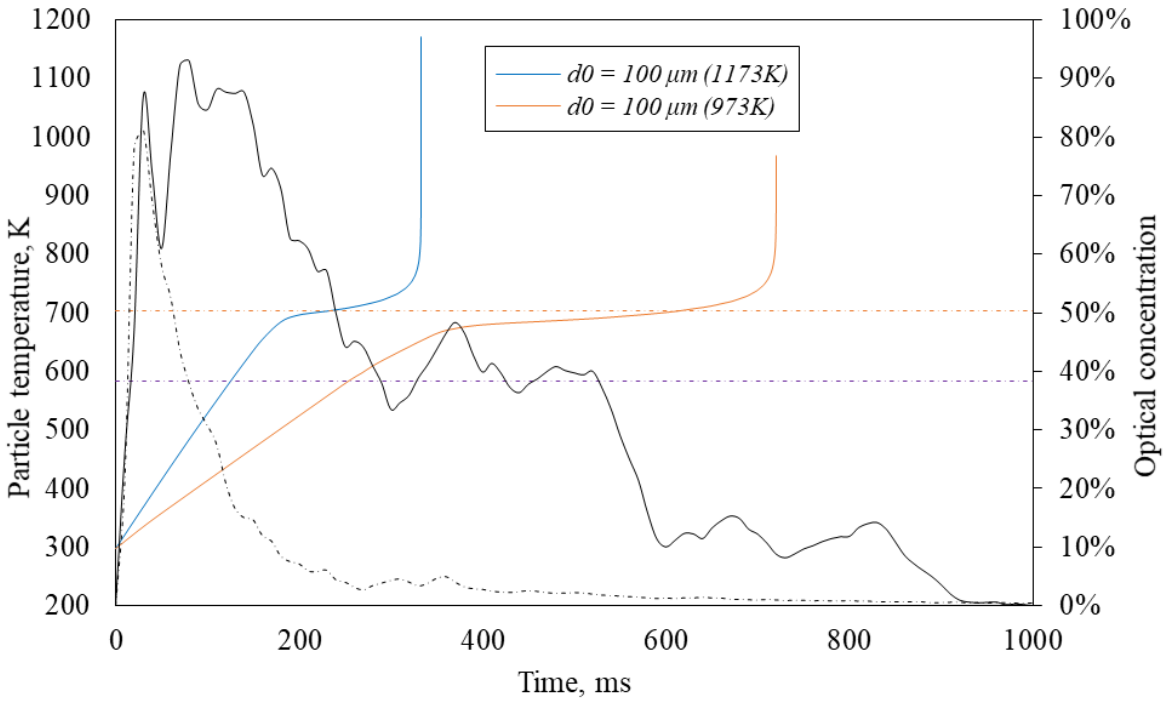

Figure 7 - Time-evolution of the particle temperature and the optical concentration obtained before and after the heated chamber (100 µm cellulose).

It must be stressed that this approach has some limitations, especially because the PSD and hydrodynamic analyses were performed on dust clouds at ambient temperature. Moreover, a dust cloud is a heterogeneous entity in space and time, which at high temperature induces a non-homogeneous temperature field, in turn leading to a non-homogeneous conversion degree of the solid phase. Furthermore, the conversion of cellulose at high temperatures forms an intermediate and sticky liquid [20,21] which may induce particle agglomeration.

3.2 Solid products

Figure 8 and Figure 9 shows the digital and SEM images of the solid residues sampled after the heated chamber during pyrolysis tests of cellulose and starch, respectively. They were chosen to be as much representative as possible of the samples collected. As expected,

essential changes in the colours of the particles can be noticed in both samples, representing the first qualitative analysis of the global conversion degree of the particles. However, the presence of white or unconverted particles also shows that pyrolysis was not complete for both powders, whatever the temperature. Such a simple and visual analysis allows for example to confirm the value of the pyrolysis onset temperature, approximately 600 K, under the conditions of a dust explosion (dispersed powder) which are different from those encountered for powder layer (e.g. by TGA).

Note the high heterogeneity in particle conversion depending on their particle size and their apparent residence time in the G-G furnace. This observation is in good agreement with the modelling and sensitivity results (Figure 11 and Figure S 6 and S 8 in Supporting information) showing that particles bigger than 100 µm need a longer residence time to be converted than the dust cloud average value measured in the modified G-G furnace.

A major difference between the thermal behaviour of starch and cellulose dust cloud is clearly perceptible by observing the SEM images. Although cellulose particles tend to form agglomerates as the reactor temperature increases, starch particles show a significantly higher tendency to create even larger clusters. This might be related to a higher formation of the liquid sticky intermediate by starch.

Moreover, the SEM imaging pointed to a modification of the particle surface morphology, as well as an increasing tendency to agglomeration/melting with the reactor temperature, which is related to a higher conversion of cellulose or starch to the intermediate liquid. The high importance of the intermediate liquid formation during cellulose pyrolysis was studied in detail by Dufour et al. [26]. This intermediate liquid even controls the global pyrolysis rate of cellulose under fast heating conditions [20, 21]. The length of the cellulose fibres is nearly unchanged when the temperature reaches 700°C, whereas it is reduced by approximately 20% and more than 50%, when the temperature rises to 800 and 900°C,

respectively. At the same time, the number of fine particles decreases significantly. Similar tests were performed also with wood powders and olive pomace and show similar trends. For instance, the visual analysis of the Douglas fir residues (Figure 10) allowed to notice that char, which is still physically attached to the wood fibres at low temperatures, tends to break away to form independent structures at 900°C. It is worth noting that char is surrounded by a layer of tar, pierced by bubbles. Aerosol release as well as tar cracking of oxygen containing compounds, which occurs from 700 to 850°C, can be responsible for such irregularities; cracking of aromatic compounds occurs at higher temperatures [28]. In parallel, the length of the fibres shortens and the residual particles agglomerate.

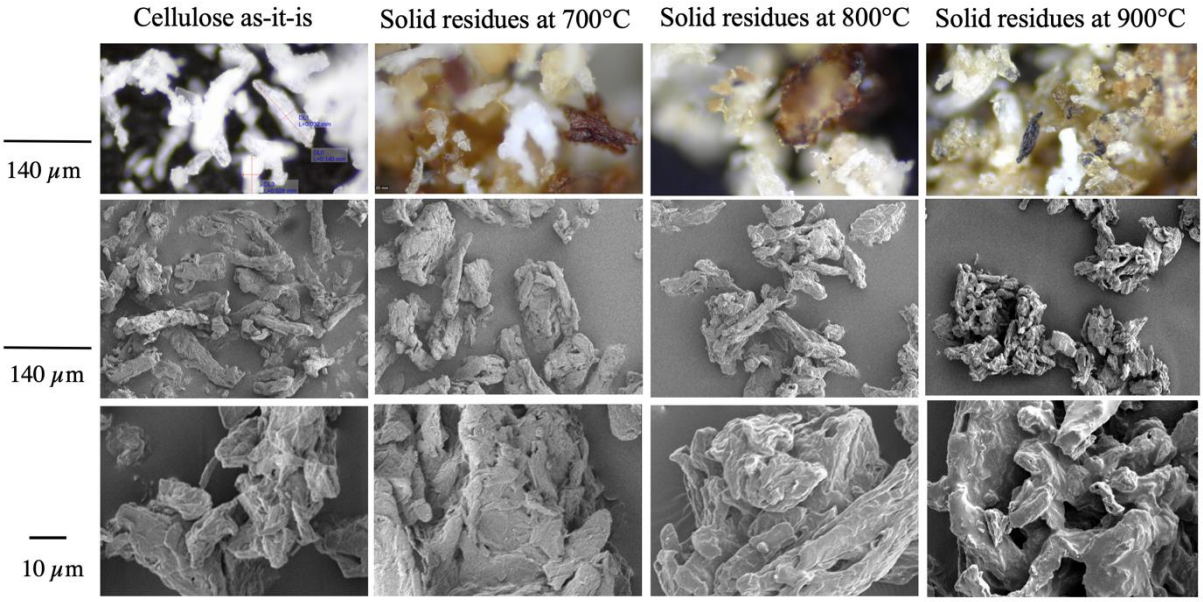

Figure 8 - Digital and SEM images of the cellulose sample (as-it-is, to the left) and the pyrolysis solid residues as a function of the furnace temperature.

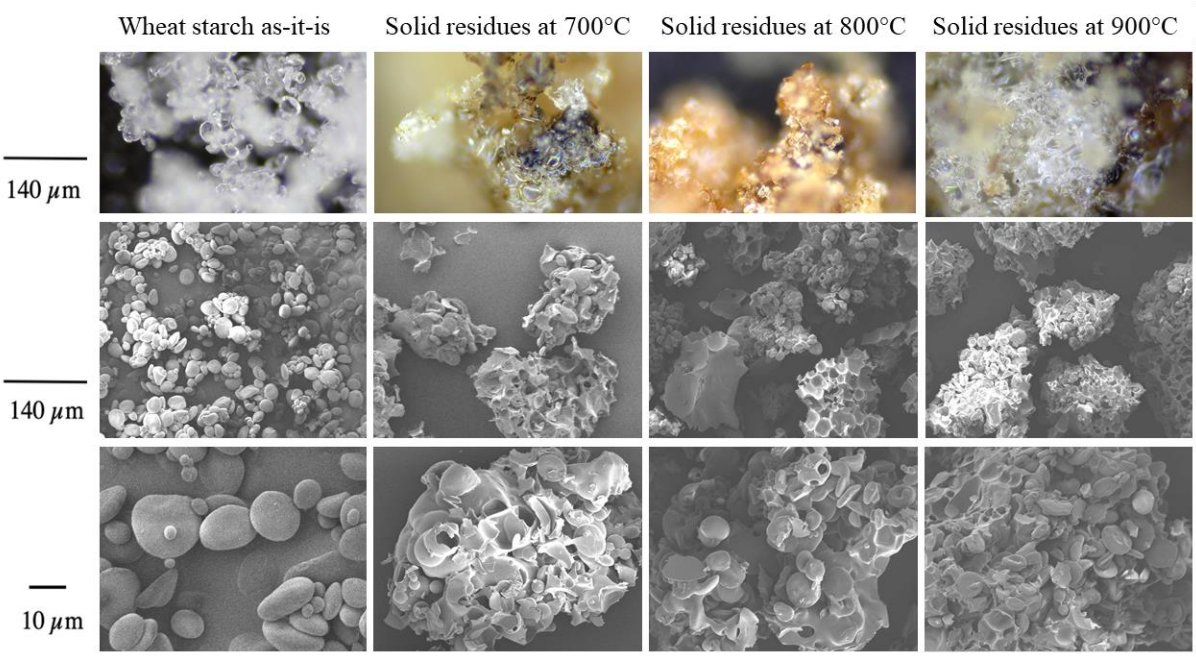

Figure 9 - Digital and SEM images of the wheat starch sample (as-it-is, to the left) and the pyrolysis solid residues as a function of the furnace temperature.

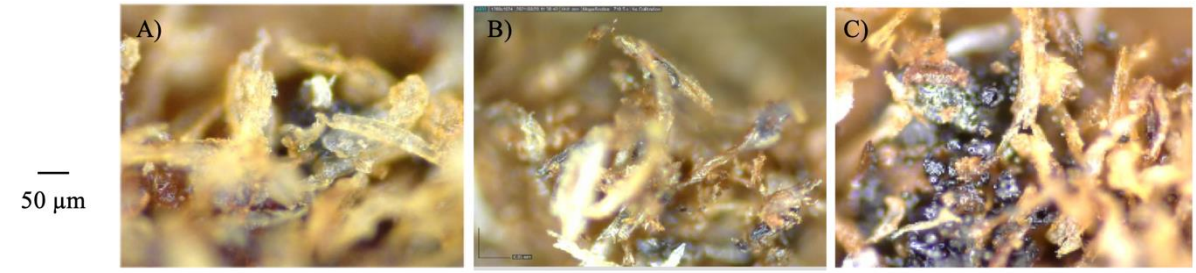

Figure 10 - Digital pictures of the solid residues collected for Douglas fir at A) 973K, B) 1073K and C) 1173K.

These results are consistent with the model. In fact, it shows (Figure 11) that even a 100 µm thick cellulose fibre would not be completely pyrolyzed after an average residence time of approximately 200 ms in the oven at 1173K (which corresponds to the average residence time determined by the high-speed video approach). Obviously, thicker particles, e.g. 200 µm fibres (i.e. cellulose agglomerates), essentially have time to heat up but not to pyrolyze for residence times below 650 ms. They might represent the white particles noticed in the microscopic observations in Figure 8.

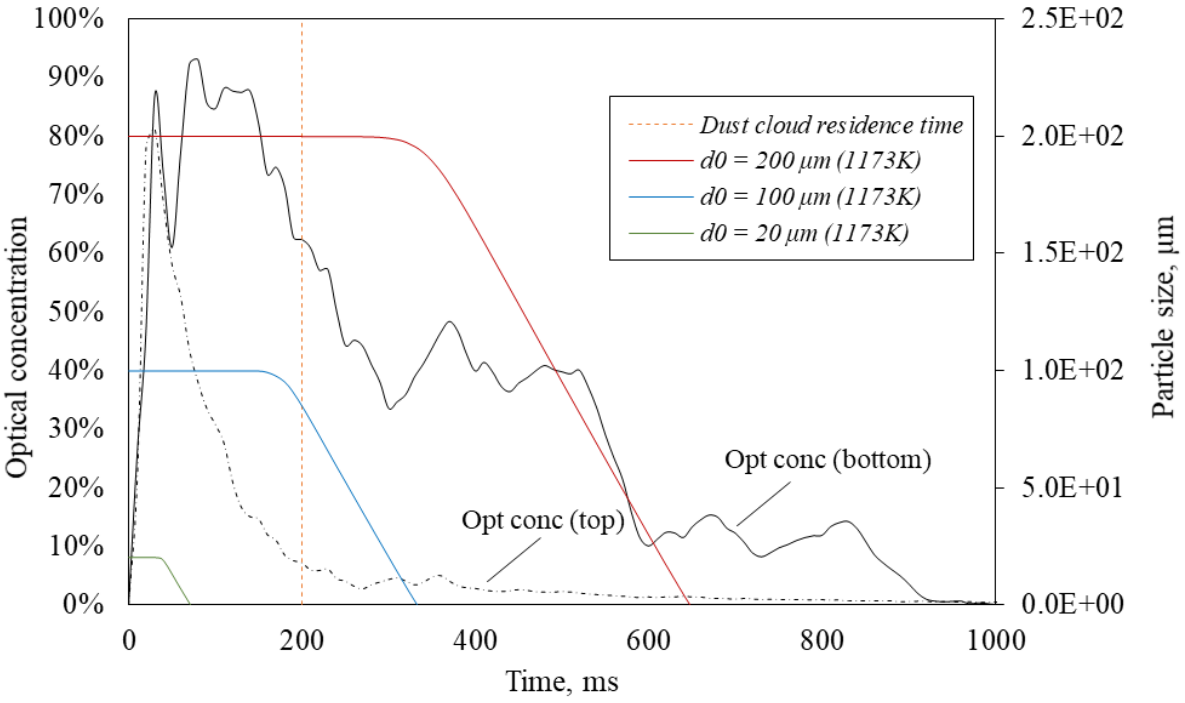

Figure 11 - Time-evolution of the particle diameter during their dispersion in the G-G furnace at 1173K, determined for three values of initial particle size (cellulose). The optical concentration was determined experimentally, before and after the heated chamber.

An attempt to quantify the global conversion of cellulose particles collected at the outlet of different reactor temperatures by comparing their volatile content (by TGA) was made. However, tests showed trivial discrepancies (see Supporting information – Figure S 9 and Figure S 10). Minor differences were noticed in the thermal behaviour of the residues regarding the onset temperatures, the mass loss and the overall trend. At the end of the analysis (at a temperature equal to 950°C), the mass volatilized in the three samples was 89.7% (standard deviation 1.4%), 94.0% (1.6%) and 92.0% (1.1%) for respectively the residue collected at 700, 800 and 900°C. The discrepancy between these results is comparable with the sensitivity of the thermo-balance, which leads to the conclusion that there was no significant difference in the volatile matter of the pyrolysis residues. Nevertheless, it should

be noted that the onset temperature of the residues appears to be slightly lower than pure cellulose (approximately 305°C), which might demonstrate a partial depolymerization of cellulose. Finally, a major difference between solid residues and raw cellulose is noticeable around 500°C. The rapid pyrolysis of the particles in the vertical chamber of the G-G furnace seems to lead only to a partial conversion of the dust cloud (especially the finer particles), which is in line with the observations given in Figure 8 and Figure 11.

To better understand the chemical conversion of cellulose as function of reactor temperature, the chemical structure of the different cellulose residues was analysed by FTIR spectroscopy. Figure 12 reports the FT-IR absorbance spectra of the cellulose pyrolysis solid residues. Three main regions were considered for the comparison of the samples. The peak around 3300 cm^{-1} corresponds to the O-H stretching associated with H-bonded hydroxyl groups [22, 23]. The intensity of the signal increased with the reactor temperature, which can be related to the increasing accessibility (i.e. an increasing vibration freedom) of the cellulose-chain OH-groups. The peak around 2900 cm^{-1} is associated with the symmetric aliphatic C-H stretching [29–31], whose intensity also increased with the reactor temperature. The last region, between 1600 and 1800 cm^{-1}, is associated with the aromatic C=C and the ketones C=O stretching. This double peak is characteristic of the presence of char, as presented by D'Acierno et al. [32], which supports the observations made from Figure 8. The increasing bands around 3300, 2900, 1400 and 1040 cm^{-1} were the typical infrared absorption carbohydrate peaks [33], which is related to depolymerized cellulose occurring in the primary pyrolysis of cellulose. Pastorova et al. [30] characterized cellulose biochars obtained at different temperatures (from 250 to 390°C) through their FTIR spectra. Three FTIR characteristic bands proposed in their work can be related to the increasing temperature. The first one is the 2800-3000 cm^{-1} region. It does not vary from 250 to 310°C but, for a reactor temperature of 390°C, the peak increases significantly, which is consistent with the spectra

shown in Figure 12. The second band is the double peak between 1600 and 1800 cm^{-1} that was also observed in this work. It steadily increases with temperature, even though the intensity of the signals between this work and Pastorova's is not of the same order of magnitude. Lastly, the peak at 1080 cm^{-1} is related to the pyranose ring skeletal vibrations, which is associated to the integrity of the cellulose. Although it is less intense than the others, in the spectra this peak's intensity decreases with the reactor temperature, showing an increasing conversion degree of the cellulosic chain.

In brief, the analysis of the solid residues allowed to identify key points of the flash pyrolysis of organic powders in suspension:

- The first step of depolymerisation of cellulosic compounds cannot be neglected when proposing reaction mechanisms;
- In comparison to cellulose, starch shows a stronger tendency to agglomerate during pyrolysis;
- For cellulose fibres larger than 100 µm, the residence time in the G-G furnace is not sufficient to achieve a high conversion rate, resulting in a low char yield.

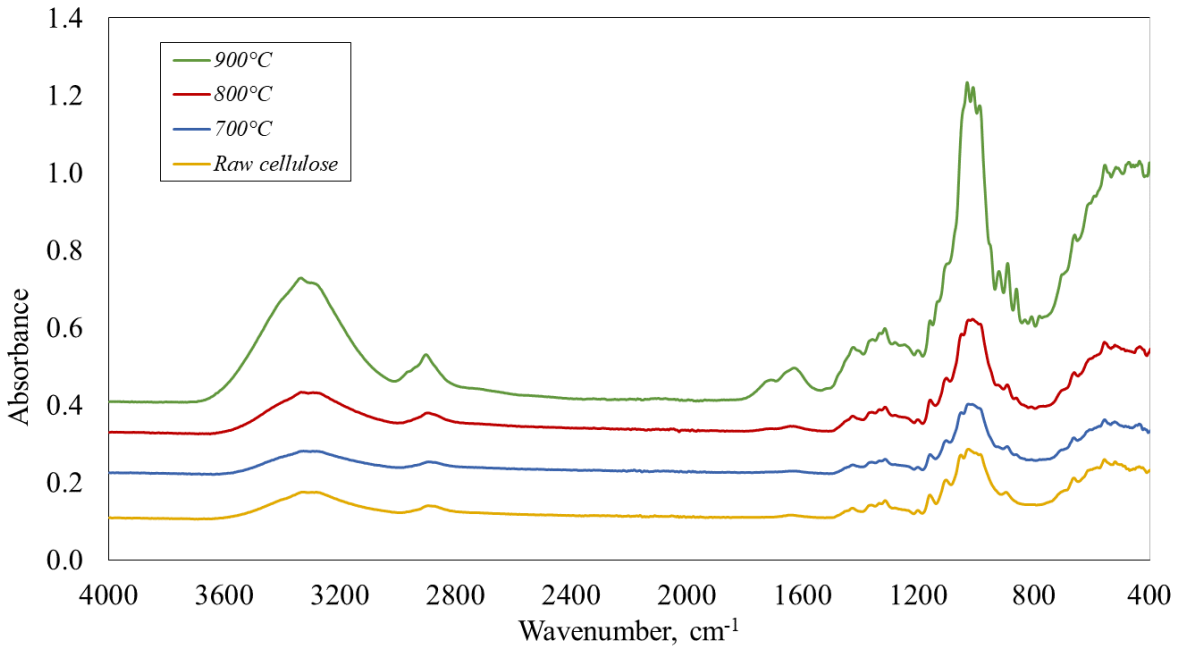

Figure 12 - FT-IR absorbance spectra of the solid residues collected after the heated chamber at a different temperature, compared to the pure cellulose.

3.3 Condensable products

Figure 13 shows the results of the GC-MS-FID on the condensable fraction. Spectra showed that the most abundant molecule was levoglucosan ($C_6H_{10}O_5$), which comes from the depolymerisation of the cellulose chain during its primary pyrolysis. Other molecules detected were acetic acid, hydroxyacetaldehyde, hydroxyacetone, dihydroxyacetone, cyclopentanepentol and 2-2-dimethoxybutane, but their concentration was much lower than those of levoglucosan. During the pyrolysis tests, the levoglucosan yield showed a peak at 800°C, which can be explained considering two concurrent phenomena: the increasing effect of the primary pyrolysis as the temperature rises and the competing secondary reaction in the gaseous phase as the temperature rises.

The behaviour observed for starch is slightly different since the concentration of hydroxyacetaldehyde was sensibly higher. However, levoglucosan remains the most important compound, and it was considered as the most representative molecule of the primary pyrolysis also for starch. Its yield is lower than the values obtained with cellulose, regardless of the temperature. The maximum yield is reached at 900°C.

Cellulose consists of a monomeric unit ($C_6H_{10}O_5$) formed from anhydrous glucose, held in place by β(1→4) glycosidic bonds [34]. This strong intra-molecular bond and the inter-chain hydrogen bonding result in the formation of a predominantly crystalline structure, leaving little room for amorphous regions. The glucopyranose-units ($C_6H_{10}O_5$) are linked by α(1→4) glycosidic bonds in starch, causing it to generally decompose at slightly lower temperatures than cellulose [35,36], but following the same pyrolytic pathway including glycoside bonds breakage [37]. Since the devolatilization of starch is easier than that of cellulose [37], the

lower production of levoglucosan can be explained either by a higher generation of non-condensable gases, or by the presence of glucose-based anhydrosugars containing two or more monomeric units, which are hardly detectable [38]. Such analysis thus enables to identify common stages but also some specificities in the pyrolysis process of biomass powders; differences and common features that can be exploited when proposing explosion mechanisms.

Under oxidizing conditions, the tar fraction undergoes oxidation reactions and thus the tar yield is lower. For both cellulose and starch, the levoglucosan yields are smaller and they are of the same order of magnitude, although they slightly increased with the temperature.

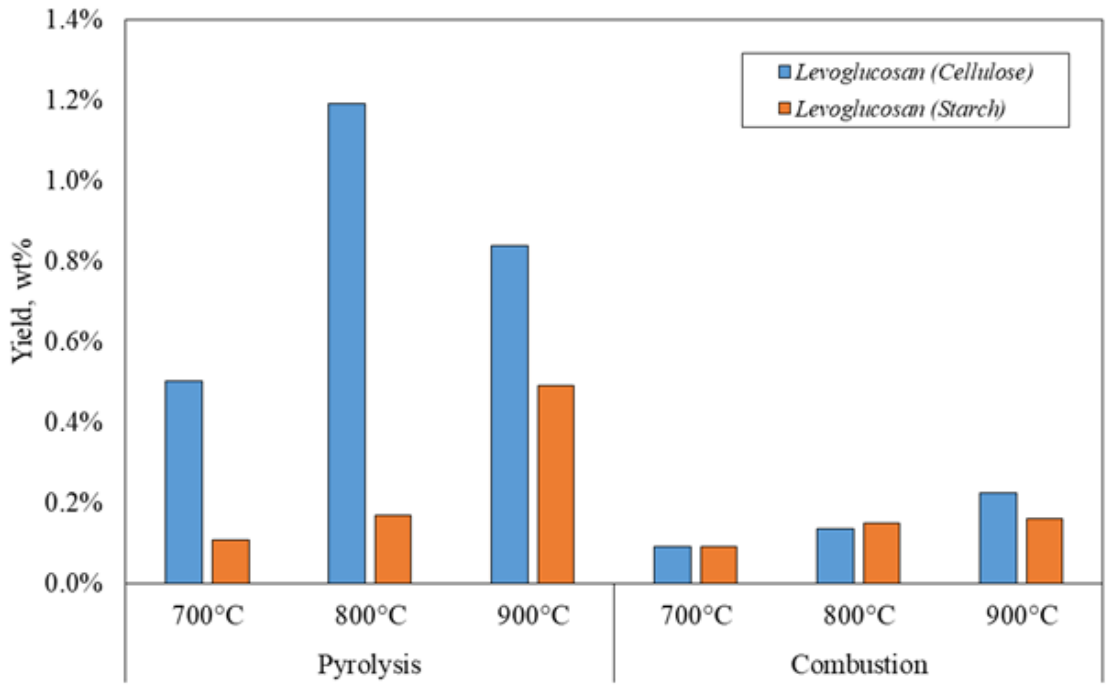

Figure 13 - The yield of the most abundant molecule in the condensable fraction, as a function of the reactor temperature, for pyrolysis and combustion tests of cellulose and starch.

3.4 Gaseous products

From the analysis of the pyrolysis gaseous products (Figure 14), CO, CO_2, H_2 and CH_4 were the most abundant species generated during the pyrolysis step and their temperature-evolution agrees with the literature [37, 39]. Other compounds, such as ethylene, were sometimes present as traces but are neglected here.

The principal components of syngas (H_2 and CO) generally increased with temperature, reaching a maximum concentration of 70 mol% (standard deviation 1%), 75 mol% (1%), 59 mol% (2%) and 73 mol% (1%) regarding the pyrolysis gases, for cellulose, wheat starch, oak and Douglas fir respectively, which is in good agreement with literature [40], although the operating conditions were different. Low yields of C_2H_4 (ethylene) and C_6H_6 (benzene - a good indicator of tertiary reactions [41]) were identified showing a slight increase as a function of the temperature. The H_2/CO ratio exhibited a linear increase and a slight reduction at 900°C for wheat starch, oak and Douglas fir, whilst the CO/CO_2 ratio increased significantly due to the higher content of CO at elevated reactor temperature (except for cellulose). Olive pomace shows a peculiar behaviour related to the complexity of its composition [42]: the CO_2 content is higher than that of CO. As the chemical composition of olive stone, especially its oxygen content, is consistent with that of other woods (approximately 43 w%), the CO_2 abundance can be explained by the composition of the wet pomace or catalytic effects due to the high mineral content.

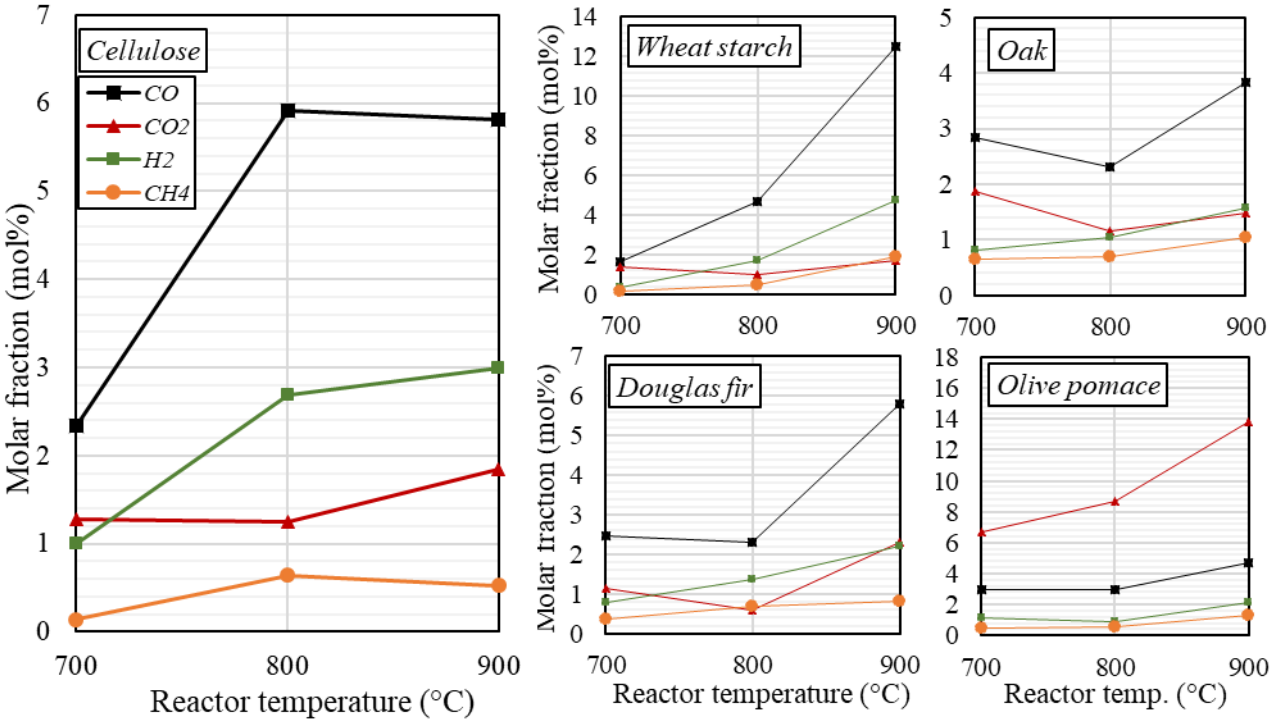

Figure 14 - Pyrolysis gases composition as a function of the powder nature and G-G furnace temperature.

Figure 15 shows the results obtained during the combustion of the powders in the G-G furnace. The methane concentration is not presented here. Its evolution is similar to hydrogen, but it is always 2 to 4 times lower. The behaviour of cellulose must be analysed independently: the CO_2/CO ratio decreases with temperature until it reaches values close to or even slightly below 1 at 1173K.

For the other organic powders, the CO_2/CO ratio increases from 973K to 1073K and then decreases or remains stable as the temperature reaches 1173K. In parallel, the hydrogen content follows an opposite evolution, with a minimum obtained at 1073K. It should be noted that the high CO_2/CO ratio obtained for oak at 1073K is essentially due to a low carbon monoxide concentration, equal to 0.4 mol%. To analyse these trends, it must be borne in mind that, unlike the endothermic phenomenon of pyrolysis for which knowledge of the furnace temperature is crucial, the exothermicity of combustion does not allow to determine the exact

temperature at which the gaseous products were generated. Indeed, the temperature of the furnace, which conditions the initiation of the pyrolysis and combustion phenomena, must not be confused with the gas-phase temperature, which is unknown here. Another essential point explaining the results shown in Figure 15 is the consideration of secondary reactions of primary volatiles (levoglucosan, furans, CO, CO_2, CH_4, H_2, etc.), which can explain both the CO and H_2 increase at a higher temperature.

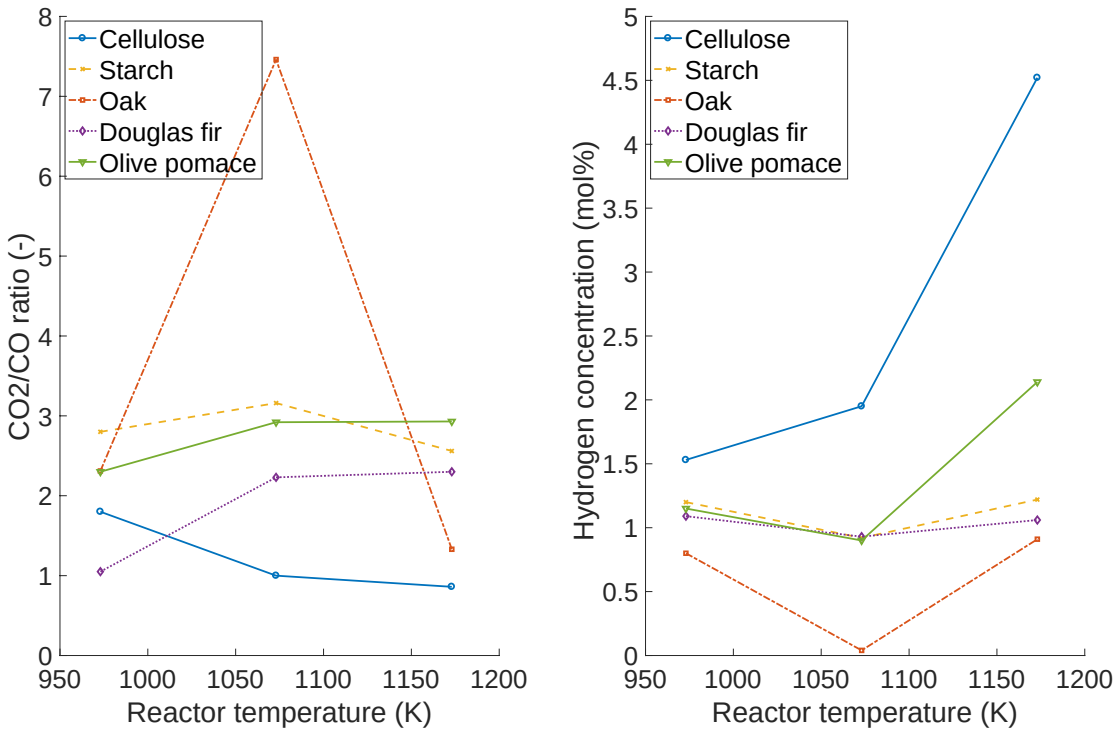

Figure 15 - Combustion gases composition (CO_2/CO ratio and hydrogen content) as a function of the powder nature and G-G furnace temperature.

3.5 Pyrolysis and combustion mechanisms for dust explosion modelling

The above analyses, carried out under both pyrolysis and combustion conditions, allow a better understanding of the reaction mechanisms playing a role during an organic dust explosion, and therefore better modelling of these phenomena.

An organic dust explosion can be schematically represented by the following subsequent stages: the heating of the particle, its pyrolysis and the homogeneous oxidation of the pyrolysis gases. Each of these steps can be decomposed into simpler phenomena, such as external and internal heat transfer, diffusive and reaction limitation. As shown the heating step can be limiting at low temperatures for large particles with a short residence time. To be able to compare pyrolysis and oxidation from a kinetic point of view, the following points should be kept in mind:

- Cellulose pyrolysis is an endothermic process, therefore the temperature of the particle during this stage changes only to a limited extent whatever the temperature of the heating source, as demonstrated in Lédé [43];
- The oxidation of pyrolysis products is an exothermic phenomenon, which results in a flame with a temperature sensibly higher than the pyrolysis temperature.

The high complexity of the global explosion phenomenon originates predominantly from the interplay between these two steps. Considering an organic particle that undergoes a pyrolysis process, it is true that the gaseous products encircling the particle can generate a flammable atmosphere, if their concentration is beyond the Lower Flammable Limit (LFL). Assuming that the gaseous mixture ignites, the flame front temperature will influence the heat flux brought to the particles and the apparent pyrolysis rate. Reversely, the volatile composition has an impact on the flame temperature and hence the overall phenomenon strictly depends on this interplay between volatile generation and oxidation. Therefore, pyrolysis and oxidation are coupled during a dust explosion. This approach is exclusively valid when a single-particle combustion is considered. For a group-combustion (low inter-particle distance, high dust concentration), the flame propagates in the direction of the cloud, which leads to the pyrolysis of the particles in the preheating zone (4-zone model: cloud, preheating zone with pyrolysis products, flame, post-combustion zone). In this case,

devolatilization/pyrolysis and oxidation, although interdependent, can be more easily distinguished. For small biomass particles, Biot (equation 3) and Damköhler (Da) numbers [44] can both be less than unity, which means that the pyrolysis is fast and homogeneous combustion controlled the dust explosion. Such behaviour has notably be observed for small octadecanol particles [44]. Considering Figure 11, the Da number of large cellulose particles (e.g. greater than 100 µm) would certainly be greater than unity under classical dust explosion conditions: the pyrolysis step should be considered as the rate-limiting step and a heterogeneous combustion is expected [45]. It is supported by the fact that, when the temperature increases, the oxidation rate increases faster than the pyrolysis rate [46].

Therefore, in Figure 16, a lumped reaction mechanism is proposed to model the cellulose pyrolysis. The experimental results in the G-G furnace were considered to select the chemical species involved. Classical oxidation reactions of the gaseous products, which are not specific to the heterogeneous reaction mechanisms of biomass (for instance, H_2, CO, C_2H_4, CH_4 oxidation reactions, water gas shift or Boudouard reactions), can then be combined with this mechanism.

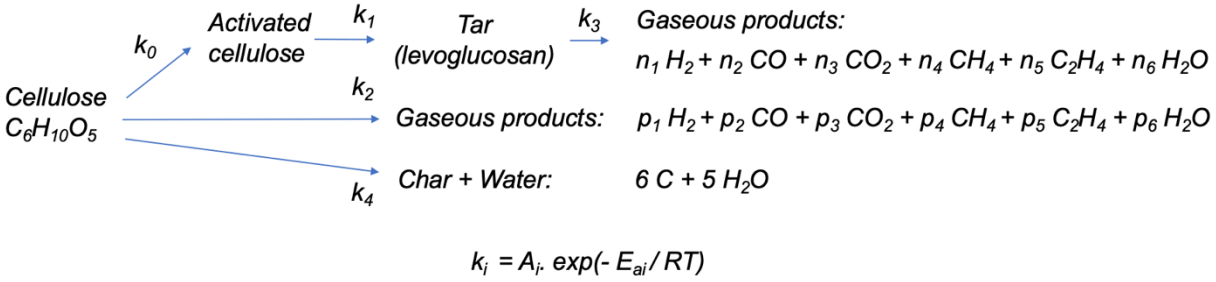

Figure 16 - Proposed reaction mechanisms to be considered during an organic dust explosion: example of cellulose.

By focusing only on the pyrolysis step, both the kinetics constants and the stoichiometric coefficients should be determined for reactions from 1 to 4 (Figure 16). Reactions corresponding to cellulose activation and tar generation can be represented using the kinetics proposed by Ranzi et al. [47]. The stoichiometric coefficients of reaction 4 are

known (6 and 5 for char and water, respectively, as reported in Ranzi et al. [47]). The remaining unknowns of the system are the twelve coefficients of reactions 2 and 3, and the six variables (A_i and $E_{a,i}$) corresponding to the Arrhenius law representing the kinetic constants k_2, k_3 and k_4. Six atomic balances can be deduced by considering the proposed reactions. For instance, considering reaction 3, for carbon, hydrogen and oxygen respectively, it is true that:

Furthermore, six equations can be deduced by considering the Godbert-Greenwald furnace a Continuously Stirred Tank Reactor (CSTR). For instance, considering carbon monoxide and hydrogen, it is true that:

$$\frac{[H_2]}{[CO]}$$

where τ is the residence time, determined experimentally and fixed at 200 ms. Ratios were determined experimentally at three different temperatures, while water-to-carbon monoxide and char-to-carbon monoxide ratios are considered unknowns at each temperature (six unknowns in total). The equations system is, hence, made of eighteen balances similar to Equations (5a), (5b) and (5c) and six equations based on atom conservation for reactions 2 and 3; it was solved using a nonlinear least-squares fitting method. Boundaries were set to avoid negative stoichiometric coefficients or unrealistic activation energies. Figure 17 describes an example of fitting for cellulose, showing a satisfactory agreement between the model based on the pyrolysis equations in Figure 16 and the experimental points in Figure 14. The stoichiometric coefficients n_i and p_i were determined, as well as the kinetic constants, providing a pyrolysis model for cellulose under dust explosion conditions. Values are reported

in Table 3 and Table 4. This model is coupled with the oxidation equations globally represented in

Figure 2. A similar fitting was successfully obtained for the other organic compounds. As can be noticed in Figure 17, the code allowed to determine the C- and the H_2O-to-CO ratios, which were not accessible experimentally. Piskorz et al. [13] reported the liquid and the insoluble solid yields as a function of the reactor temperature. Water and C follow the same trend as presented in their work, slightly increasing and strongly decreasing with the temperature.

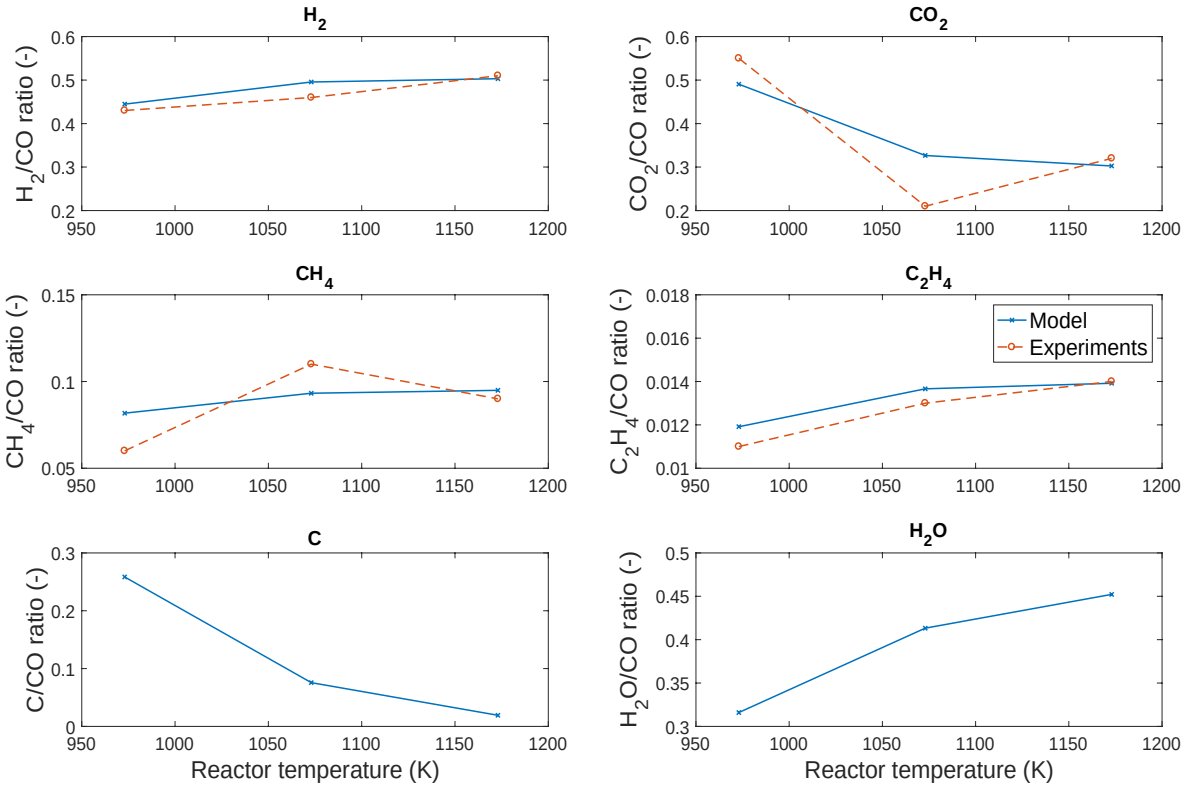

Figure 17 - Comparison between the pyrolysis model developed and the experimental gas/CO ratios.

Table 3 - Stoichiometric coefficients calculated with the fast cellulose pyrolysis model for cellulose dust explosions.

Reaction	**H_2**	**CO**	**CO_2**	**CH_4**	**C_2H_4**	**H_2O**
Levoglucosan to gaseous products (Reaction 3)	0.93	1.84	0.55	0.17	0.03	0.86

Cellulose to gaseous products (Reaction 2)	0.86	2.38	1.8	0.15	0.02	1.48

Table 4 - Activation energies and pre-exponential factors determined with the fast cellulose pyrolysis model for cellulose dust explosions. T is the temperature in K.

Reaction	**E_a, J.mol^{-1}**	**A, s^{-1}**
Cellulose to levoglucosan (Reaction 0 + 1) [47]	$1 \cdot 10^4$	$4 \cdot T$
Levoglucosan to gaseous products (Reaction 3)	$2 \cdot 10^5$	$1 \cdot 10^{16}$
Cellulose to char and water (Reaction 4)	$7 \cdot 10^4$	$4 \cdot 10^{10}$
Cellulose to gaseous products (Reaction 2)	$1 \cdot 10^4$	$1 \cdot 10^8$

Figure 18 andTable 5 show a comparison between the kinetic constants determined with the model proposed in this work and with two others frequently used in the literature, also dedicated to cellulose flash pyrolysis [48,49]. Ranzi et al. [48] mainly based its model on thermo-gravimetric analysis, while Piskorz et al. [49] employed a fluidised bed to study the cellulose flash pyrolysis. Figure 18 shows significant differences between the different kinetic constants and demonstrates how an experimental technique's operating conditions influence the kinetic parameters. If the deviations are large over the whole temperature range considered, it is necessary to focus on the range of this study, i.e. from 973 to 1173K. The three constants determined are globally higher than those proposed in the literature, in particular for the reactions R3 and R4.

The kinetics of direct generation of non-condensable gases from cellulose (R2) seems to be relatively unaffected by temperature variation. This evolution is consistent with the observations made in this study: small cellulose particles volatilize rapidly, from 700°C, and generate little tar. An increase in temperature hardly modifies the reactivity of the small cellulose particles. However, the direct conversion of larger fibres into non-condensable gas is difficult and becomes the rate-limiting step as the temperature increases. As for the

volatilization of tar proposed in this work (R3), it is increasingly favoured by a temperature rise. Specifically, levoglucosan-related secondary reactions are very slow at low temperatures, as known and well documented for low heating rates [50]. The experimental results confirm the enhancement of this mechanism at high temperatures: the amount of tar decreases, more gases are generated and the presence of bubbles/cracks on the surface of the tar shows the production of gases or aerosols.

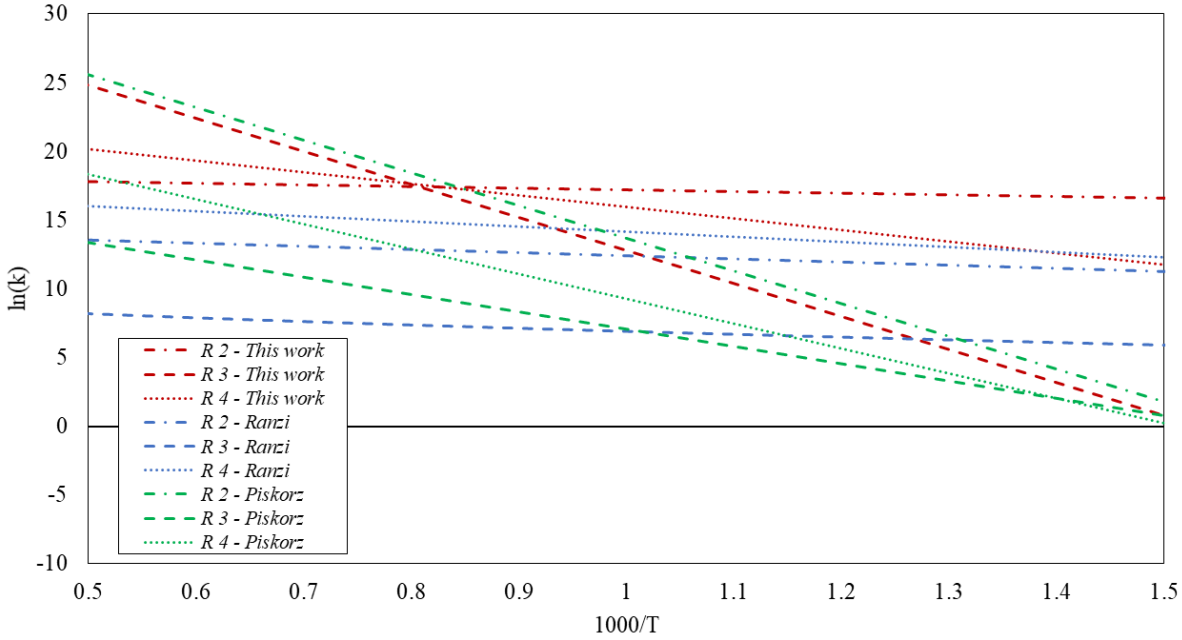

Figure 18 - Comparison between the kinetic constants obtained in this work and those reported in Ranzi et al. [48] and Piskorz et al. [49]

Table 5 - Lumped flash pyrolysis reactions considered for the comparison in Figure 18

References	Reaction R2	Reaction R3	Reaction R4
Ranzi et al. [48]	Activated cellulose → Gases and volatiles	Activated cellulose → Levoglucosan	Cellulose → Char and water
Piskorz et al. [49]	Activated cellulose → Volatiles	Tar and gases → Gases	Activated cellulose → Char and gases

This work	Cellulose → Gases	Levoglucosan → Gases	Cellulose → Char and water

4. Conclusions

The thermal behaviour of six biomass powders, as well as their pyrolysis and combustion mechanisms, were studied using a Godbert-Greenwald furnace. Modelling results and experimental data show that various rate-limiting steps can be observed for the same dust sample, as a function of its particle size distribution. For cellulose and wood samples having a D90 greater than 100 µm, the residence time of their large particles in the G-G furnace is too short to reach their pyrolysis temperature: their explosion kinetics will be governed by their heating rate. On the other hand, these samples exhibiting a D10 close to 20 µm, their small particles will be converted rapidly (less than 100 ms), leading to fast generation of pyrolysis gases. In such case, the organic dust cloud can be considered as a hybrid mixture of combustible gases and unburnt solids. Although composed of small particles, the influence of heterogeneous reactions during starch combustion cannot be ruled out as, during their pyrolysis, starch particles form sticky intermediates which lead to the generation of large clusters.

Although there are similarities, particularly with regard to the significant influence of the depolymerisation step and the generation of levoglucosan, both the gases and the mechanisms observed differ between this study, carried out under the conditions relevant for dust explosion, and the studies carried out on dust layers or non-powdered materials. The low proportion of char in the solid residue is a notable difference from low heating rates pyrolysis processes, as well as the predominance of levoglucosan-related secondary reactions at high temperatures.

This study, carried out at high heating rates on powders in suspension in a turbulent environment, leads to the development of a lumped-kinetic model, based on 5 reactions and adapted to cellulose explosions. Significant differences were observed between the kinetic constants proposed by this approach and those available in the literature and determined by TGA or fluidised bed, demonstrating how an experimental technique's operating conditions influence the kinetic parameters.

List of symbols

d_p = particle diameter, m

L = particle mean length, m

ρ_s = cellulose density, $kg.m^{-3}$

C_p = specific heat capacity, $J.kg^{-1}.K^{-1}$

T_p = particle temperature, K

k = thermal conductibility, $W.m^{-1}.K^{-1}$

F = view factor, -

ε = emissivity, -

σ = Stefan-Boltzmann constant, $W.m^{-2}.K^{-4}$

T_w = wall temperature, K

h = convective heat transfer coefficient, $W.m^{-2}.K^{-1}$

ΔH_p = pyrolysis reaction enthalpy, $J.kg^{-1}$

k_p = pyrolysis reaction kinetic constant, s^{-1}

E_a = pyrolysis reaction activation energy, $J.mol^{-1}$

A = pyrolysis reaction pre-exponential factor, s^{-1}

Declaration of interests

☒ The authors declare that they have no known competing financial interests or personal relationships that could have appeared to influence the work reported in this paper.

☐The authors declare the following financial interests/personal relationships which may be considered as potential competing interests:

References

[1] Islas A, Fernández AR, Betegón C, Martínez-Pañeda E, Pandal A. Computational Assessment of Biomass Dust Explosions in the 20L Sphere. Process Saf Environ Prot 2022:S0957582022006371. https://doi.org/10.1016/j.psep.2022.07.029.

[2] Azam S, Mishra DP. Effects of particle size, dust concentration and dust-dispersion-air pressure on rock dust inertant requirement for coal dust explosion suppression in underground coal mines. Process Saf Environ Prot 2019;126:35–43. https://doi.org/10.1016/j.psep.2019.03.030.

[3] Tan X, Schmidt M, Zhao P, Wei A, Huang W, Qian X, et al. Minimum ignition temperature of carbonaceous dust clouds in air with CH4/H2/CO below the gas lower explosion limit. Fuel 2020;264:116811. https://doi.org/10.1016/j.fuel.2019.116811.

[4] Bu Y, Yuan Y, Xue S, Amyotte P, Li C, Yuan W, et al. Effect of admixed silica on dispersibility of combustible dust clouds in a Godbert-Greenwald furnace. Powder Technol 2020;374:496–506. https://doi.org/10.1016/j.powtec.2020.07.071.

[5] Mittal M, Guha BK. Study of Ignition Temperature of a Polyethylene Dust Cloud. Fire Mater 1996;20:97–105. https://doi.org/10.1002/(SICI)1099-1018(199603)20:2<97::AID-FAM568>3.0.CO;2-L.

[6] Mittal M, Guha BK. Minimum ignition temperature of polyethylene dust: a theoretical model. Fire Mater 1997;21:169–77. https://doi.org/10.1002/(SICI)1099-1018(199707/08)21:4<169::AID-FAM604>3.0.CO;2-Y.

[7] Chen T, Van Caneghem J, Degrève J, Berghmans J, Verplaetsen F, Vanierschot M. Comparison between a numerical model and the classic thermal explosion theories for the calculation of the minimum ignition temperature of dust clouds. Process Saf Environ Prot 2022;166:222–31. https://doi.org/10.1016/j.psep.2022.08.022.

[8] Xu S, Liu J, Cao W, Li Y, Cao W. Experimental study on the minimum ignition temperature and combustion kinetics of coal dust/air mixtures. Powder Technol 2017;317:154–61. https://doi.org/10.1016/j.powtec.2017.04.059.

[9] Addai EK, Gabel D, Krause U. Models to estimate the minimum ignition temperature of dusts and hybrid mixtures. J Hazard Mater 2016;304:73–83. https://doi.org/10.1016/j.jhazmat.2015.10.015.

[10] Liu A, Chen J, Lu X, Li D, Xu W. Influence of components interaction on pyrolysis and explosion of biomass dust. Process Saf Environ Prot 2021;154:384–92. https://doi.org/10.1016/j.psep.2021.08.032.

[11] Li Q, Wu Q-Y, Jiang W, Qian J-Y, Zhang L, Wu M, et al. Effect of pulsed electric field on structural properties and digestibility of starches with different crystalline type in solid state. Carbohydr Polym 2019;207:362–70. https://doi.org/10.1016/j.carbpol.2018.12.001.

[12] ISO/IEC 80079-20-2. Explosive atmospheres - Part 20-2: Material characteristics - Combustible dusts test methods. 2016.

[13] Piskorz J, Majerski P, Radlein D, Vladars-Usas A, Scott DS. Flash pyrolysis of cellulose for production of anhydro-oligomers. J Anal Appl Pyrolysis 2000;56:145–66. https://doi.org/10.1016/S0165-2370(00)00089-9.

[14] Greene GA, Finfrock CC, Jr TFI. Total hemispherical emissivity of oxidized Inconel 718 in the temperature range 300±1000°C. Exp Therm Fluid Sci 2000:9.

[15] Lédé J, Authier O. Temperature and heating rate of solid particles undergoing a thermal decomposition. Which criteria for characterizing fast pyrolysis? J Anal Appl Pyrolysis 2015;113:1–14. https://doi.org/10.1016/j.jaap.2014.11.013.

[16] Dufour A, Girods P, Masson E, Rogaume Y, Zoulalian A. Synthesis gas production by biomass pyrolysis: Effect of reactor temperature on product distribution. Int J Hydrog Energy 2009;34:1726–34. https://doi.org/10.1016/j.ijhydene.2008.11.075.

[17] Pu Y, Hu F, Huang F, Davison BH, Ragauskas AJ. Assessing the molecular structure basis for biomass recalcitrance during dilute acid and hydrothermal pretreatments. Biotechnol Biofuels 2013;6:15. https://doi.org/10.1186/1754-6834-6-15.

[18] Zoghlami A, Paës G. Lignocellulosic Biomass: Understanding Recalcitrance and Predicting Hydrolysis. Front Chem 2019;7:874. https://doi.org/10.3389/fchem.2019.00874.

[19] Lu K, Hao N, Meng X, Luo Z, Tuskan GA, Ragauskas AJ. Investigating the correlation of biomass recalcitrance with pyrolysis oil using poplar as the feedstock n.d.:28.

[20] Chua YW, Wu H, Yu Y. Effect of cellulose–lignin interactions on char structural changes during fast pyrolysis at 100–350 °C. Proc Combust Inst 2021;38:3977–86. https://doi.org/10.1016/j.proci.2020.08.014.

[21] Salem Z, Lebik H, Cherafa WK, Allia K. Valorisation of olive pits using biological denitrification. Desalination 2007;204:72–8. https://doi.org/10.1016/j.desal.2006.04.025.

[22] GmbH S, Pulverhaus A. LASER-DIFFRACTION RESULTS FROM DYNAMIC IMAGE ANALYSIS DATA n.d.:4.

[23] Mishra DP, Azam S. Experimental investigation on effects of particle size, dust concentration and dust-dispersion-air pressure on minimum ignition temperature and combustion process of coal dust clouds in a G-G furnace. Fuel 2018;227:424–33. https://doi.org/10.1016/j.fuel.2018.04.122.

[24] Dufour A, Castro-Diaz M, Brosse N, Olcese R, Bouroukba M, Snape C. In Situ Analysis of Biomass Pyrolysis by High Temperature Rheology in Relations with H-1 NMR. Energy Fuels 2012;26:6432–41.

[25] Boutin O, Ferrer M, Lédé J. Radiant flash pyrolysis of cellulose—Evidence for the formation of short life time intermediate liquid species. J Anal Appl Pyrolysis 1998;47:13–31. https://doi.org/10.1016/S0165-2370(98)00088-6.

[26] Dufour A, Ouartassi B, Bounaceur R, Zoulalian A. Modelling intra-particle phenomena of biomass pyrolysis. Chem Eng Res Des 2011;89:2136–46. https://doi.org/10.1016/j.cherd.2011.01.005.

[27] Boutin O, Ferrer M, Lédé J. Flash pyrolysis of cellulose pellets submitted to a concentrated radiation: experiments and modelling. Chem Eng Sci 2002;57:15–25. https://doi.org/10.1016/S0009-2509(01)00360-8.

[28] Vreugdenhil BJ, Zwart RWR. Tar formation in pyrolysis and gasification n.d.:38.

[29] Janu R, Mrlik V, Ribitsch D, Hofman J, Sedláček P, Bielská L, et al. Biochar surface functional groups as affected by biomass feedstock, biochar composition and pyrolysis temperature. Carbon Resour Convers 2021;4:36–46. https://doi.org/10.1016/j.crcon.2021.01.003.

[30] Pastorova I. Cellulose char structure : a combined analytical Py-GC-MS, F IR, and NMR study. Carbohydr Res 1994:21.

[31] Behazin E, Ogunsona E, Rodriguez-Uribe A, Mohanty AK, Misra M, Anyia AO. Mechanical, Chemical, and Physical Properties of Wood and Perennial Grass Biochars for Possible Composite Application 2016:16.

[32] D'Acierno F. Sustainable biochars from carbonization of cellulose filaments and nanocrystals 2021:7.

[33] Wang J. Effect of pyrolysis conditions on levoglucosan yield from cotton straw and optimization of levoglucosan extraction from bio-oil. J Anal Appl Pyrolysis 2016:10.

[34] Li L, Rowbotham JS, Christopher Greenwell H, Dyer PW. An Introduction to Pyrolysis and Catalytic Pyrolysis: Versatile Techniques for Biomass Conversion. New Future Dev. Catal., Elsevier; 2013, p. 173–208. https://doi.org/10.1016/B978-0-444-53878-9.00009-6.

[35] Mischnick P, Momcilovic D. Chemical Structure Analysis of Starch and Cellulose Derivatives. Adv. Carbohydr. Chem. Biochem., vol. 64, Elsevier; 2010, p. 117–210. https://doi.org/10.1016/S0065-2318(10)64004-8.

[36] Zong P, Jiang Y, Tian Y, Li J, Yuan M, Ji Y, et al. Pyrolysis behavior and product distributions of biomass six group components: Starch, cellulose, hemicellulose, lignin, protein and oil. Energy Convers Manag 2020;216:112777. https://doi.org/10.1016/j.enconman.2020.112777.

[37] Fu P, Yi W, Bai X, Li Z, Hu S, Xiang J. Effect of temperature on gas composition and char structural features of pyrolyzed agricultural residues. Bioresour Technol 2011;102:8211–9. https://doi.org/10.1016/j.biortech.2011.05.083.

[38] Moldoveanu SC. Chapter 7. Analytical pyrolysis of polymeric carbohydrates. Tech. Instrum. Anal. Chem., vol. 20, Elsevier; 1998, p. 217–315. https://doi.org/10.1016/S0167-9244(98)80028-0.

[39] Sun S, Tian H, Zhao Y, Sun R, Zhou H. Experimental and numerical study of biomass flash pyrolysis in an entrained flow reactor. Bioresour Technol 2010;101:3678–84. https://doi.org/10.1016/j.biortech.2009.12.092.

[40] Wei L, Xu S, Zhang L, Zhang H, Liu C, Zhu H, et al. Characteristics of fast pyrolysis of biomass in a free fall reactor. Fuel Process Technol 2006:9.

[41] Anthony Dufour, Eric Masson, P. Girods, Yann Rogaume, A. Zoulalian. Evolution of Aromatic Tar Composition in Relation to Methane and Ethylene from Biomass Pyrolysis-Gasification. Energy Fuels 2011;25:4182–9. https://doi.org/10.1021/ef200846g.

[42] Bartocci P, D'Amico M, Moriconi N, Bidini G, Fantozzi F. Pyrolysis of Olive Stone for Energy Purposes. Energy Procedia 2015;82:374–80. https://doi.org/10.1016/j.egypro.2015.11.808.

[43] Lédé J. Reaction temperature of solid particles undergoing an endothermal volatilization. Application to the fast pyrolysis of biomass. Biomass Bioenergy 1994;7:49–60. https://doi.org/10.1016/0961-9534(94)00046-V.

[44] Gao W, Mogi T, Yu J, Yan X, Sun J, Dobashi R. Flame propagation mechanisms in dust explosions. J Loss Prev Process Ind 2015;36:186–94. https://doi.org/10.1016/j.jlp.2014.12.021.

[45] Pang L, Cao J, Zhao Y, Yuan C, Yang K, Zhang Z. Minimum ignition energy of LDPE dust/ethylene hybrid mixture. J Loss Prev Process Ind 2021;72:104546. https://doi.org/10.1016/j.jlp.2021.104546.

[46] Speight JG. Combustion of hydrocarbons. Handb. Ind. Hydrocarb. Process., Elsevier; 2020, p. 421–63. https://doi.org/10.1016/B978-0-12-809923-0.00010-2.

[47] Ranzi E, Faravelli T, Manenti F. Pyrolysis, Gasification, and Combustion of Solid Fuels. Adv. Chem. Eng., vol. 49, Elsevier; 2016, p. 1–94. https://doi.org/10.1016/bs.ache.2016.09.001.

[48] Ranzi E, Debiagi PEA, Frassoldati A. Mathematical Modeling of Fast Biomass Pyrolysis and Bio-Oil Formation. Note I: Kinetic Mechanism of Biomass Pyrolysis. ACS Sustain Chem Eng 2017;5:2867–81. https://doi.org/10.1021/acssuschemeng.6b03096.

[49] Piskorz J, Radlein DStAG, Scott DS, Czernik S. Liquid Products from the Fast Pyrolysis of Wood and Cellulose. In: Bridgwater AV, Kuester JL, editors. Res. Thermochem. Biomass Convers., Dordrecht: Springer Netherlands; 1988, p. 557–71. https://doi.org/10.1007/978-94-009-2737-7_43.

[50] Ranzi E, Cuoci A, Faravelli T, Frassoldati A, Migliavacca G, Pierucci S, et al. Chemical Kinetics of Biomass Pyrolysis. Energy Fuels 2008;22:4292–300. https://doi.org/10.1021/ef800551t.